

Research Article

The curved uncut chip thickness model: A general geometric model for mechanistic cutting force predictions

David Hajdu^{a,b,*}, Asier Astarloa^c, Istvan Kovacs^d, Zoltan Dombovari^{a,b}^a MTA-BME Lendület Machine Tool Vibration Research Group, H-1111 Budapest, Hungary^b Department of Applied Mechanics, Faculty of Mechanical Engineering, Budapest University of Technology and Economics, Muegyetem rkp. 3., H-1111 Budapest, Hungary^c Ideko - Member of BRTA, Dynamics & Control Department, Elgoibar, Basque Country, Spain^d Fogaskerékgvár Ltd., H-2890 Tata, Hungary

ARTICLE INFO

Keywords:

Curved uncut chip thickness
Nose radius
Cutting force

ABSTRACT

The curved uncut chip thickness model is introduced to predict the cutting forces for general uncut chip geometries using the mechanistic approach. Classical geometric models assume that the cutting force is distributed along straight elementary sections of the uncut chip area, which has limited physical validity, but makes mathematical treatments easier for simple cases. The new model assumes that the flow of the material on the contact area of the tool is given by a continuous vector field, according to which the curved uncut chip thickness is measured. The cutting force is distributed along these paths, which leads to a mathematically unique and consistent solution for regular and complex cutting edge geometries. These curved paths can be generated by basic mechanical models, which mimic the more realistic motion of the chip segments along the rake face, without the need of explicit time-consuming cutting simulations. The presented computational procedure generalizes cutting force prediction based on geometric parameters, orthogonal cutting data and the orthogonal to oblique transformations only. The effectiveness of the model for various cutting edge geometries (e.g., thread turning inserts) under extreme cutting conditions is presented in case studies, laboratory and industrial experiments.

1. Introduction

Prediction of cutting forces in machining operations is an important part of process planning, since it determines the power consumption of the machine, the required torque during cutting, the static deformation of the tool, surface quality of the workpiece, accuracy, stability, and other factors. Accurate modeling of the real mechanics behind the cutting process is, however, very challenging due to the intricate nature of chip formation and physical behavior of the material under cutting conditions. Still nowadays, numerical simulations are typically too complicated and time-consuming, or just not reliable enough to replace experimental cutting operations performed on the selected material with the specific tools (see, e.g., finite element models of chip formation processes [1,2]). Therefore, researchers and manufacturing engineers rather rely on the orthogonal cutting database [3], and predict the cutting forces for general machining operations considering the technological parameters assuming straight (line) chip thickness and an appropriate discretization in the ‘width of the chip’ along the

cutting edge. These geometric assumptions are, however, inconsistent in general, and it is not trivial which model predicts better real cutting forces.

Khoshdarregi and Altintas [4] presented that classical geometric models can lead to ‘chip interference’ in the computation of cutting forces, which highlights the inconsistency of the solutions. There are two critical assumptions in the literature that lead to problems in classical models:

- The uncut chip area is divided into straight sections, which are normal to the cutting edge (this also gives the direction of the elemental forces). This leads to interference along the curved cutting edges.
- The orientation of the straight chip segments are computed by geometric (algebraic) equations only, which omit the physical model.

* Corresponding author at: Department of Applied Mechanics, Faculty of Mechanical Engineering, Budapest University of Technology and Economics, Muegyetem rkp. 3., H-1111 Budapest, Hungary.

E-mail address: hajdu@mm.bme.hu (D. Hajdu).

<https://doi.org/10.1016/j.ijmactools.2023.104019>

Received 7 December 2022; Received in revised form 13 April 2023; Accepted 17 April 2023

Available online 6 May 2023

0890-6955/© 2023 The Author(s). Published by Elsevier Ltd. This is an open access article under the CC BY-NC-ND license (<http://creativecommons.org/licenses/by-nc-nd/4.0/>).

Nomenclature

h	uncut chip thickness (m)
a	depth of cut (m)
b	chip width (m)
α_n	rake angle (rad)
λ_s	inclination angle (rad)
η	chip flow angle (rad)
τ_s	shear stress (Pa)
ϕ_n	shear angle (rad)
β_a, β_n	average and projected friction angles (rad)
T, R	transformation matrix and rotation matrix
$A, \Delta A$	area and elementary area (m ²)
P_r	reference plane
P_a	face plane
f	feed (mm or mm/rev)
γ_f	side rake angle (rad)
γ_p	back rake angle (rad)
κ_r	lead angle (rad)
v_f	feed velocity (secondary motion, m/min)
v_c	cutting speed (primary motion, m/min)
n	rake face normal vector
D	diameter (m)
n	spindle speed (rpm)
r_ϵ	nose radius (m)
ϵ	nose angle (rad)
x, y, z	global coordinate system (c.s.)
t, r, a	orthogonal c.s. (tangential, radial, axial)
$\tilde{t}, \tilde{r}, \tilde{a}$	cutting edge c.s.
v, \tilde{r}, \tilde{a}	rake face c.s.
u, w, v	chip flow c.s.
$f_j(h)$	specific cutting force function (N/m)
$K_{j,c}$	cutting coefficient (N/m ²)
$K_{j,e}$	edge coefficients (N/m)
$F_j(h)$	cutting force components (N)
F	cutting force vector (N)
C	compliance matrix (m/N)
$A_j(a, h)$	weight function
$\delta(a)$	Dirac-delta function
r_c	chip compression ratio
C_0, C_1	constants (rad)
φ	rotation angle (rad)
r, s, t	natural coordinate system
U, V, W	nodal displacements
N_i	shape functions
g, \tilde{g}	vector fields
B	strain–displacement matrix
E	material matrix
J	Jacobian matrix
K^e, K	elemental stiffness matrix and global stiffness matrix
U	vector of nodal displacements
N_e	number of triangular mesh elements
N_k	number of edge elements
N_n	number of nodes

On one hand, the Poisson burr and the side flow effect are counterexamples that show the local non-normal flow of material during the fabrication process (see the work of Li et al. [5]). These phenomena

suggest that classical models are not acceptable in all of the cases. On the other hand, since the chip formation is a physical process, it must have a unique solution that follows the behavior of material, not solely algebraic equations. Based on the reasoning above, we conclude that the chip flow paths cannot be modeled generally by straight lines.

Therefore, in this paper we present the concept of the curved uncut chip thickness model, which generalizes the application of the mechanistic approach in case of complex cutting edge geometries. The curved paths of the model should mimic the motion of the material along the contact area of the tool, however, this is either not available, or multi-physics finite element simulations would be needed. In order to solve this issue, at this stage of the research, we employ a mesh-based discretization of the uncut chip area and use the solution of a linear partial differential equation to generate a vector field, which is compatible with predefined constraints. It is important to highlight that the curved uncut chip thickness model does not simulate directly the chip formation process, instead, it utilizes a physical (mathematical) model which provides a vector field related to a possible motion of the chip. The presented model does not completely satisfy all requirements, but boundary conditions and modeling assumption can be updated if we have more information about the real physical process. The improved models will not change the fact that the uncut chip thickness is measured along the curved sections. Alternatively, any vector field can be implemented in the model, which approximates the chip flow along the surface of the tool. The other advantage of the proposed model is that it can cooperate with orthogonal cutting data and orthogonal to oblique transformation, which makes it implementable by using already known empirical cutting models [3]. Thus, in summary this work proposes the following novel approach:

- A mathematically consistent, unique curved uncut chip thickness model is introduced.
- The unique streamline of curved uncut chip thickness model is calculated by employing a low-DOF linear simple compressed solid model constrained at the current cutting edge and unconstrained along the past and free cut surfaces.
- Along the curved uncut chip thickness linear or nonlinear cutting force characteristics can be applied.
- Along the curved uncut chip thickness orthogonal to oblique transformation can be utilized using the local oblique angles determined from the geometry and the solution of the model.

In this manner, by using the proposed methodology, the complex geometry of multi-tooth thread cutting inserts, serrated milling cutters and broaching tools can be dealt generally. Specifically, in this study, metric and trapezoidal thread turning inserts are tested in experiments to highlight the effect of modeling approaches.

The complex studies in this paper reveal that the classical modeling approaches fail to uniquely discretize the uncut chip area in complex cases, and hence the solutions are not trivial. The new proposed method overcomes the problem of chip interference by taking into account the physical flow of chip segments along the rake face of the tool. With use of the new model, moderate improvement can be reached for high-feed cutting operations, and significant difference can be observed at technologically extreme conditions. The presented experiments highlight the need of advanced models for special or intense cutting operations.

The structure of the paper is as follows. In the rest of Section 1, a brief literature review is given on the most commonly used cutting force models, and the orthogonal to oblique transformation is presented for defining the used variables and parameters. Section 2 introduces the new approach based on the curved uncut chip thickness model. The geometrical model and comparisons are presented in short case studies. Laboratory and industrial experiments are presented in Sections 3 and 4, and finally, results are concluded in Section 5.

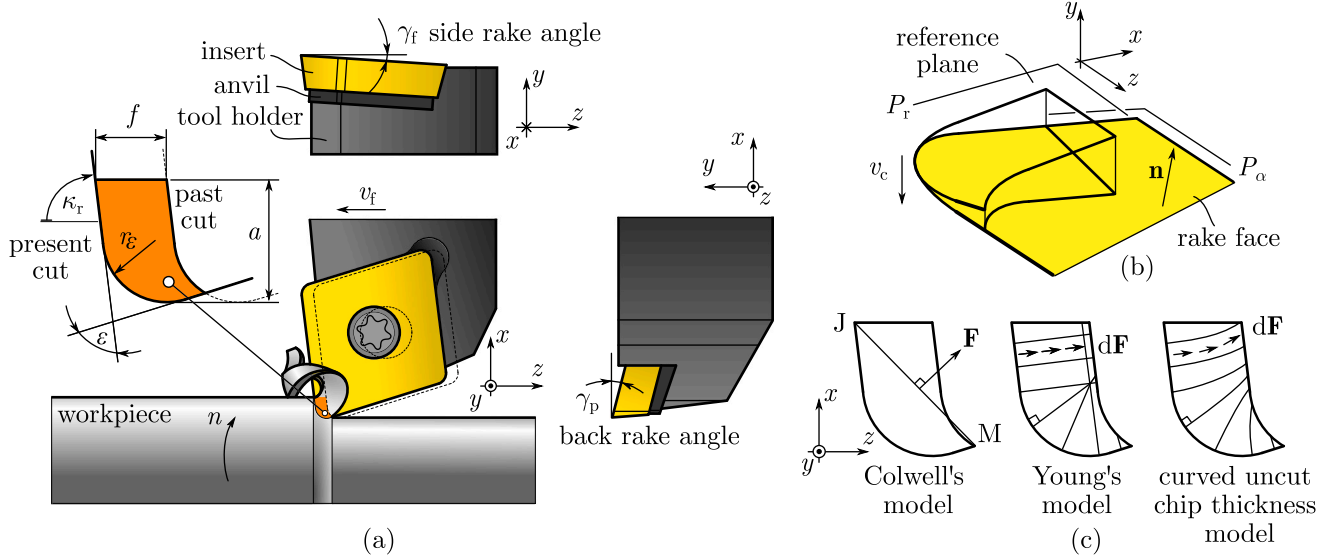


Fig. 1. Cutting force prediction for tools with nose radius in case of turning operation. (a) Tool geometry. (b) 3D view of the uncut chip area on the reference plane and its projection to the rake face. (c) Direction of the cutting force suggested by the different models in case of orthogonal cutting ($\gamma_p = 0^\circ$ and $\gamma_f = 0^\circ$).

1.1. Review of existing works

The modeling of chip formation can be considered the core of the metal cutting theory. According to Astakhov [6], the basic mechanics of the single-shear plane model are known since the observations of the cutting process that were presented by Time (1870) [7]. Tresca (1873) [8] suggested that the chip removal was based on the compression of the material ahead of the tool. However, further work by Time (1877) [9] provided evidences that the material being cut is rather deformed by shearing rather than compression. Some years later a physical explanation of the shearing process was proposed by Zvorykin (1896) [10]. Although these simplified models were not capable of describing the three-dimensional chip generation, they sat the basis for the modeling of the chip formation, leading to more complex models based on the mechanics of chip flow.

A widely used model has been presented by Merchant [11,12] for orthogonal cutting in 1945, where the primary shear zone is a thin plane, and the cutting edge is perfectly sharp. The aim is to predict the cutting forces based on the essential data only (such as the shear plane angle, friction angle, shear stress, and geometrical data), and omit the complicated phenomena. The model of Merchant allows one to approximate cutting characteristics based on simple algebraic calculations. Later, in 1951, Lee and Shaffer [13] introduced the slip-line model considering the laws of plasticity, which assumes that the material is rigid-plastic, and the shear-plane is quasi-static with slip-lines being parallel to and perpendicular to the shear plane [14]. These models were extended further to describe the real deformation better, e.g., considering the effect of work-hardening, edge radius, strain rate, or heat generation [15]. For a more detailed review on the topic, see the work of Germain et al. [16].

The analytical models are not capable to handle the effect of complicated geometries, nose radius or chip breaker grooves [3]. A mechanistic approach offers an alternative solution, which requires a parameter identification based on cutting experiments performed with the selected workpiece-cutter combination. As a result of orthogonal cutting experiments, the cutting force characteristics (as the function of the uncut chip thickness) can be determined. This methodology assumingly makes it possible to predict cutting forces for more complicated tool edge geometries, such as tools with considerable nose radius [17], see Fig. 1. However, still, it would not take into account the effect of chip breaker grooves.

The first model, which considers the effect of nose radius originates from Colwell [18], who investigated orthogonal cutting operations already in 1954. In that model, it is assumed that the chip flow direction is perpendicular to the equivalent chord connecting the surface and the side points of the edge engagement (J-M points in Fig. 1c), while the the magnitude of the cutting force is proportional to the total uncut chip area. Due to the simplicity and applicability of the approach, this assumption has been adopted by many researchers in the past. Bus et al. [19] compared the predictions to experiments, while Hu et al. [20] and Wen et al. [21] extended the method to oblique cutting operations. The assumptions have been implemented by Eynian et al. [22], who used the equivalent chord to predict unstable self-excited (*chatter*) vibrations.

Although the prediction of Colwell works reasonably well in practice, it is difficult to generally accept that the direction of the chip flow is determined only by the side-points of the engagement edge curve. Instead, Okushima and Minato [23] suggested in 1959 to use an averaged chip flow direction based on the nearly orthogonal cutting conditions. Since in classical orthogonal cutting, the chip flow direction is normal to the cutting edge, the average of the elementary chip flow angles along the cutting edge can be used to predict the averaged chip flow direction.

In order to generalize the geometrical models and find a better description of the cutting force direction, Young et al. [24] proposed a new method in 1987, see Fig. 1c. Young's approach suggests that the elementary chip flow direction along the cutting edge is normal to the edge (as in Okushima's method), the elementary friction force is normal to the edge and the magnitude is determined by the equivalent uncut chip thickness and elementary uncut chip area. The solution is, however, not unique, since the geometric assumptions are only valid close to the cutting edge. The total uncut chip area is subdivided into such segments, which are bounded by straight lines and perpendicular to the local cutting edge. Each segment is viewed as an elementary orthogonal classical cutting, and the resultant force is the sum of elementary cutting forces. This approach has been adopted the most in the literature, and found to be reliable for practical applications, however, it fails in case of general uncut chip geometries. Close to the curved cutting edges, the intersections of the lines produce interference, which is not acceptable in the models [4].

The results of Young have been extended by Wang and Mathew [25] and later by Arsecularatne et al. [17,26] to tools with nonzero

inclinations angles by introducing equivalent cutting edges to trace back the calculation to classical models. Regenerative machine tool vibrations are predicted based on these approaches by Totis and Sortino [27] and by Kuster and Gygax [28] for internal turning, and by Totis for milling operations [29], too. The predictions have been deeply studied in the literature, experiments are performed and compared to the theoretical models by Lazoglu et al. [30], Atabey et al. [31,32], Kaymakci et al. [33], and by several other researchers.

Young's method (and its extensions) also has limitations, e.g., the assumption that the local chip flow direction is always perpendicular to the corresponding cutting edge produces interference (self-intersecting lines) in general. It is not always trivial how to split the area into straight segments, which matter of choice and its physical reason are completely arbitrary. Khoshdarregi and Altintas [4] presented a method, which keeps the segments straight, but lets the segments tilt to avoid the inconsistent scenarios. The method is presented for threading, where the application of Young's method often runs into such difficulties. This extension of Young's model, however, still does not guarantee that the solution is mathematically unique, more specifically the results depend on user's choice to start the iterative process described or to tune the numerical parameters in the algorithms.

The differences between the predictions of the above mentioned models have been studied by Wang et al. [34], Kouadri et al. [35] and Wu et al. [36], just to mention a few. It is often demonstrated that the calculations are typically acceptable, but measurements are often found to be somewhere in between the suggestions of Colwell and Young.

In order to approach the solution from a different perspective, nonlinear multi-physics finite element (FE) simulations also have been investigated in the past. While the potential in such simulations is not questionable, there are many physical and numerical parameters in the model, which have to be adjusted properly to provide accurate and reliable predictions. The determination of the parameters of the constitutive models (e.g., Johnson–Cook) requires various mechanical tests and specific experimental setups, as shown by Cheng et al. [37]. Since these tests cannot always be executed, the data is often taken from references, which may significantly deviate even for the same material (see, e.g., the collection of identified model parameters for IN718 given in the work of Ozel et al. [2]). The applied simulation method (e.g., Lagrangian or Coupled Eulerian Lagrangian (CEL) approach) and element size, shape or orientation all have effect on the final results, as presented by Xu et al. [38]. Moreover, the detailed friction modeling between the tool and material interface is also a problem, as shown by Arrazola and Ozel [1]. Several experimental comparisons are presented by the above mentioned references (e.g., Wu et al. [36] showed studies for chip breakage tests, Afazov et al. [39] for micro-milling cutting force predictions, or Ozel et al. [2] for face turning tests), however, the accuracy is not guaranteed in general as the result of many uncertain factors. Due to the complexity of simulations, the complete FE-based solutions are far to fully replace experimental cutting tests. This fact excludes the use of simulation in industrial production-oriented applications.

By introducing the curved uncut chip thickness model, we can cover a wider spectrum of applications and can overcome the difficulties generated by the complicated geometries. It is assumed that the cutting force is normal to the cutting edge close to the edge, but then it bends to avoid chip interference (self-intersecting lines), mimicking the real mechanical chip flow path on the rake face. Since the flow of the material is a complicated physical phenomenon, it is not possible to predict accurately the cutting force based on geometrical models only. Therefore, we create an artificial vector field from a mechanical model, which fulfills the above mentioned criteria and can be a better approximation for the local flow directions. The details of the model are presented in Section 2.

1.2. Cutting tool geometry

An external turning tool with a single point insert is presented in Fig. 1a,b, which is used for demonstration purposes. The cutting force models are applicable for milling, drilling, broaching, planing and other non-abrasive machining operations, by modifying the description of geometry and (or) coordinate system. The tool moves in the direction of the feed (z) with constant (secondary) speed v_f , while the feed in one revolution is f (given in mm or mm/rev). The workpiece rotation n is given in rpm, which gives the (primary) cutting speed $v_c(\text{m/min}) = D\pi n$, where D is the diameter of the workpiece. The depth of cut a is measured in radial direction x . The lead angle is κ_r , while γ_f and γ_p are the side- and back rake angles of the tool, respectively. The insert has a nose radius r_n , and nose angle ϵ . The coordinate system (x, y, z) in Fig. 1 is standard for turning operations, which is the coordinate system of the machine (and can be different for other machines or cutting operations). In the example (Fig. 1), the normal vector of the rake face is determined by the side and back rake angles as

$$\mathbf{n} = \begin{bmatrix} 0 \\ -\sin \gamma_f \\ \cos \gamma_f \end{bmatrix} \times \begin{bmatrix} \cos \gamma_p \\ -\sin \gamma_p \\ 0 \end{bmatrix}. \quad (1)$$

Considering the geometrical data of the tool (edge angles, nose radius, normal vector, etc.), the edge engagement can be defined. Due to simplicity, the chip breakers on the rake face are omitted, and the surface is assumed to be completely flat (the normal vector is constant along the rake face).

1.3. Specific cutting force models

As it is mentioned above, the new model is based on classical assumptions made on orthogonal and oblique cutting operations. In this short subsection we recall the classical cutting force models and orthogonal to oblique transformation (Fig. 2) in order to apply it later for the curved uncut chip thickness model.

If the cutting force components are needed to be defined in the global coordinate system of the machine, then the forces must be transformed from one coordinate system to the other. In order to describe the force components and transformations concisely, the following coordinate systems (c.s.) and notations are applied:

- (0) machine c.s. (x, y, z),
- (1) orthogonal c.s. (t, r, a),
- (2) cutting edge c.s. ($\bar{t}, \bar{r}, \bar{a}$),
- (3) rake face c.s. (v, \bar{r}, \bar{a}),
- (4) chip flow c.s. (v, w, u).

The coordinate systems are presented in Fig. 2. Note that the tangential direction (t) is parallel to the direction of the cutting velocity (the radial (r) and axial (a) directions are normal to it), while the chip flow direction u is defined on the rake face and v is normal to the rake face.

Transformation between the different coordinate systems in oblique cutting can be described by the rotation matrices

$$\mathbf{R}_{1,\eta} = \begin{bmatrix} 1 & 0 & 0 \\ 0 & \cos \eta & -\sin \eta \\ 0 & \sin \eta & \cos \eta \end{bmatrix}, \quad (2)$$

$$\mathbf{R}_{2,\alpha_n} = \begin{bmatrix} \cos \alpha_n & 0 & \sin \alpha_n \\ 0 & 1 & 0 \\ -\sin \alpha_n & 0 & \cos \alpha_n \end{bmatrix}, \quad (3)$$

$$\mathbf{R}_{3,\lambda_s} = \begin{bmatrix} \cos \lambda_s & -\sin \lambda_s & 0 \\ \sin \lambda_s & \cos \lambda_s & 0 \\ 0 & 0 & 1 \end{bmatrix}, \quad (4)$$

where 1,2,3 indicate the axis of rotation ($1 = t, x$; $2 = r, y$; $3 = a, z$, etc.), λ_s is the inclination angle, α_n is the rake angle, and η is the chip flow angle measured on the rake face, moreover, the positive direction of

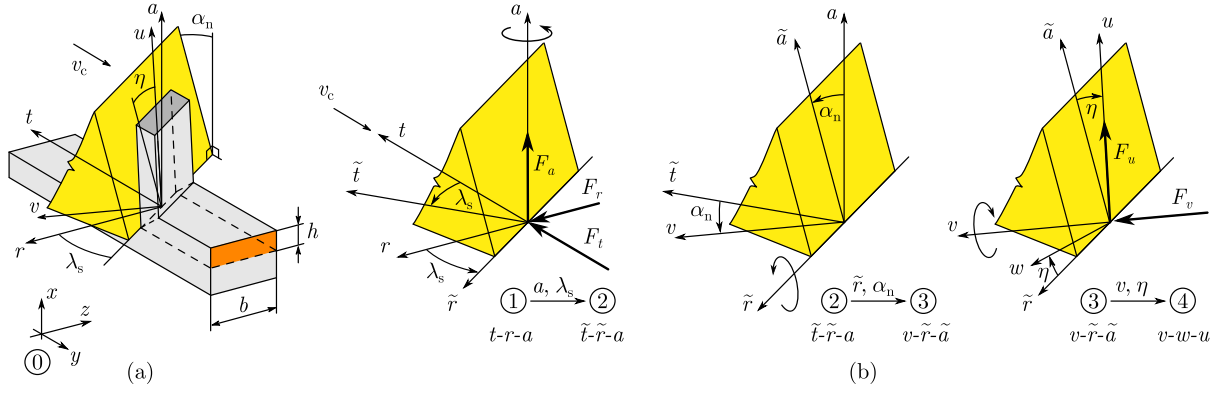


Fig. 2. The orthogonal to oblique transformation [3]. (a) Coordinate systems in oblique cutting operation. (b) Transformation from coordinate system 1 to 4.

rotation is defined around the positive direction of the corresponding axis. For instance, the transformation between c.s. 1 and 4 is written as

$$\mathbf{T}_{4,1} = \mathbf{R}_{3,\lambda_s} \mathbf{R}_{2,\alpha_n} \mathbf{R}_{1,\eta}, \quad (5)$$

where the sequence of multiplications follows intrinsic rotations, i.e., rotations occur in the local frame of reference in the order $a - \tilde{r} - v$. The indices (4, 1) in $\mathbf{T}_{4,1}$ indicate that $\mathbf{T}_{4,1}$ transforms the basis vectors of c.s. 1 to the basis vectors of c.s. 4. (see Fig. 2b).

Cutting force components are typically characterized by empirical formulas, which are (linear or nonlinear) functions of at least the uncut chip thickness h . The specific cutting forces are formulated generally as $\mathbf{f}(h) = [f_t(h), f_r(h), f_a(h)]^T$ or $\mathbf{f}(h) = [f_v(h), 0, f_u(h)]^T$, depending on the coordinate system [3]. These characteristics are either determined by orthogonal cutting tests having $f_j(h)$ using the mechanistic approach, or they can be predicted theoretically using material properties and the engineering database [3]. One of the simplest model assumes $f_j(h)$ in the form

$$f_j(h) = K_{jc}h + K_{je}, \quad j = u, v, \text{ or } j = t, a, r, \quad (6)$$

where K_{jc} is cutting coefficient and K_{je} is the edge coefficient. Note that the cutting characteristics may appear as a linear function of the uncut chip thickness h , however, $K_{jc}(h)$ can also be nonlinear (e.g., titanium alloys [3]). It is an important remark here that the effect of edge radius is not investigated in details, but its effect is assumed to be included in the characteristics $f_j(h)$ either by the edge coefficient or as a nonlinear function of the uncut chip thickness.

The orthogonal to oblique transformation is utilized to predict the elementary cutting coefficients K_{jc} in the chip flow c.s. ($j = u, v$) [3,33] in the form

$$K_{uc} = \frac{\tau_s \sin \beta_a \sqrt{1 + \tan^2 \eta \sin^2 \beta_n}}{\cos \lambda_s \sin \phi_n \sqrt{\cos^2(\phi_n + \beta_n - \alpha_n) + \tan^2 \eta \sin^2 \beta_n}}, \quad (7)$$

$$K_{vc} = \frac{\tau_s \cos \beta_a \sqrt{1 + \tan^2 \eta \sin^2 \beta_n}}{\cos \lambda_s \sin \phi_n \sqrt{\cos^2(\phi_n + \beta_n - \alpha_n) + \tan^2 \eta \sin^2 \beta_n}},$$

where τ_s is the shear stress of the workpiece material, ϕ_n is the shear angle, $\tan \beta_n = \tan \beta_a \cos \eta$, moreover β_n is called the projected friction angle, and β_a is the average friction angle. For simplicity, we follow Stabler's rule, which means that $\eta = \lambda_s$ is fixed [40].

The pressure distribution along the rake face is often modeled empirically, which can be taken into account by a theoretical weight function $\Lambda_j(a, h)$, which satisfies the condition

$$\int_0^h \Lambda_j(a, h) da = 1, \quad j = u, v. \quad (8)$$

Standard formulas presented in this section express the cutting characteristics in terms of the uncut chip thickness h and the uncut chip width

b measured on the reference plane (see Fig. 2a). Therefore, the cutting force vector $\mathbf{F} = [F_t, F_r, F_a]^T$, is defined theoretically in the form

$$\mathbf{F} = \int_0^b \int_0^h \mathbf{T}_{4,0} \begin{bmatrix} \Lambda_v(a, h) f_v(h) \\ 0 \\ \Lambda_u(a, h) f_u(h) \end{bmatrix} da dr. \quad (9)$$

Since the elementary cutting force vectors are aligned parallel to each other, the integral simplifies to $F_j = b f_j(h)$, where $j = t, r, a$. Also note that the distribution does not affect the force magnitudes if the elementary chip segments are straight. However, in case of the curved uncut chip thickness model, the weight functions Λ_j can have effect. Note that if the distribution is assumed to be uniform, then $\Lambda_j = 1/h$, which again gives $F_j = b f_j(h)$ from (9).

2. The curved uncut chip thickness model

The first step to determine the curved uncut chip segments is to generate a vector field, along which the chip is assumed to flow on the rake face. This curved chip uncut thickness (see Fig. 3) allows using empirical cutting force characteristics described in Section 1.3. For this purpose, we create a hypothetical low-resolution, simple finite element plate model defined over the uncut chip area with uniform thickness and compress it normal to its plane. This actually mimics the tangential inertial pressure and its effect on the arriving chip segments. The nodal solution is used for generating a vector field to derive the chip flow path directions and consequently the geometry of the curved uncut chip thickness. The consequence of the model is that its solution is

- mathematically unique, because the calculation is based on a linear finite element model, which has only one solution, and
- free of inconsistency, i.e., the curved uncut chip segments do not intersect each other (there is no interference).

2.1. Modeling approach

The vector field generating the curved uncut chip thickness on the reference plane is calculated from a linear low-resolution mesh-based model without any real chip formation simulation. We use a simplified isoparametric triangular element (see Appendix A), which models a plate with uniform thickness, and only uniform compression normal to its plane is allowed. The advantage of such a simplified element is the fast numerical computation and the easy implementation. The displacements are only constrained at the nodes along the cutting edge, while the load is a displacement-driven compression in the normal direction of the reference plane. The numerical calculation procedure is presented in details in Appendix A, while a sample solution is shown in Fig. 3. The deformation gradient on the reference plane (x, z in the machine coordinate system) produces the vector field $\mathbf{g}(x, z) = [g_x, 0, g_z]^T$, along which the curved uncut chip thickness is defined.

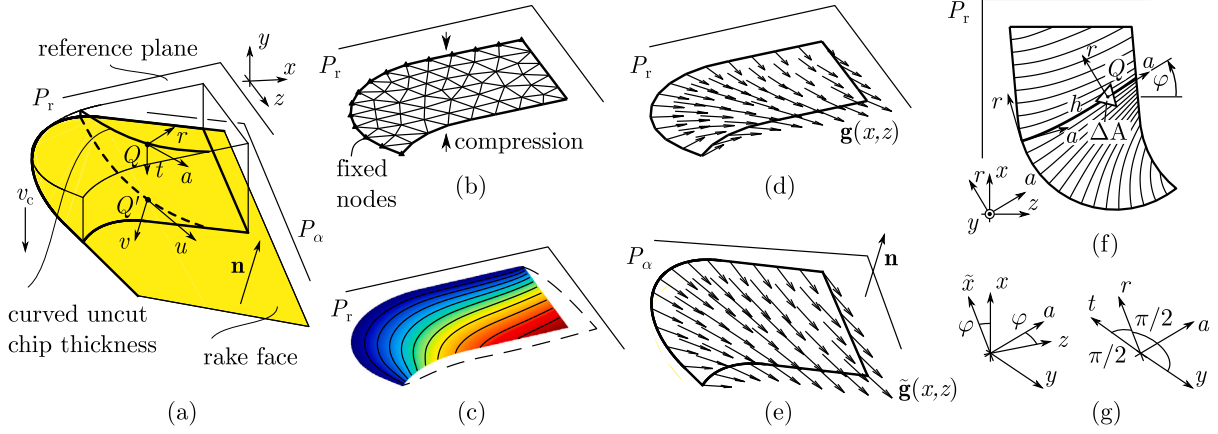


Fig. 3. Generation of the curved uncut chip segments. (a) 3D view of the uncut chip geometry. (b) Finite element mesh (nodes are fixed on the cutting edge, the load is a compression in direction y). (c) Nodal displacement magnitudes calculated from the deformed shape. (d) Displacement gradient $\mathbf{g}(x, z)$ (gradient is normal to the cutting edge on the reference plane). (e) vector field transformed to rake face following Stabler's rule and the local rake and inclination angles. (f) Curved chip segments generated by the trajectories of the vector field $\mathbf{g}(x, z)$ on the reference plane. (g) Transformation from the global c.s. (x, y, z) to the local c.s. (t, r, a) .

Note that the boundary conditions and the model can be updated if we have more information about the real physical process, however, it does not affect the concept (and computation) of the curved uncut chip thickness model.

If the side and back rake angles are nonzero, then the equivalent rake angles α_n and inclination angles λ_s are different at every point along the rake face. Therefore, rotation matrices are applied to describe the transformation from the reference plane to the rake face. The aim is to treat the cutting process locally as an equivalent oblique cutting. First, we determine the angle between the gradient \mathbf{g} and axis z , denoted by φ , which is

$$\tan \varphi = \frac{g_x}{g_z}. \quad (10)$$

The corresponding local rake angle and inclination angle are determined from the constraint that the normal vector $\mathbf{n} = [n_x, n_y, n_z]^T$ of the rake face is known. In order to describe the rotations correctly, the transformation matrix $\mathbf{T}_{4,0}$ must be determined, which transforms the unit base vector $[1, 0, 0]^T$ from the c.s. 0 to c.s. 4. This transformed vector is parallel with the normal vector of the plane, i.e.,

$$\mathbf{T}_{4,0} \begin{bmatrix} 1 \\ 0 \\ 0 \end{bmatrix} = \begin{bmatrix} -\sin \alpha_n \sin \varphi + \cos \alpha_n \cos \varphi \sin \lambda_s \\ -\cos \alpha_n \cos \lambda_s \\ -\sin \alpha_n \cos \varphi - \cos \alpha_n \sin \varphi \sin \lambda_s \end{bmatrix} \equiv -\mathbf{n}, \quad (11)$$

where

$$\mathbf{T}_{4,0} = \mathbf{R}_{2,\varphi} \mathbf{R}_{3,-\pi/2} \mathbf{T}_{4,1} \quad (12)$$

is the transformation considering the definition of coordinate systems (see Figs. 2 and 3f,g). Since the transformation from one normal vector to the other contains the unknown angles, then (11) can be solved, that is, α_n and λ_s are calculated as

$$\sin \alpha_n = n_x \sin \varphi + n_z \cos \varphi \quad \text{and} \quad \sin \lambda_s = \frac{n_z - \cos \varphi \sin \alpha_n}{\cos \alpha_n \sin \varphi}. \quad (13)$$

Since these angles for relevant technological parameters are relatively small, the inverse of the sine function gives the correct angles of rotations. Note that the solution can be singular if $\sin \varphi = 0$ ($\cos \varphi = \pm 1$), in this case (11) is solved again and the solution (13) is replaced by

$$\sin \alpha_n = n_z \cos \varphi \quad \text{and} \quad \sin \lambda_s = \frac{-n_x}{\cos \alpha_n \cos \varphi}. \quad (14)$$

Also note that if Stabler's rule is followed [40], then the chip flow angle η is equal to the local inclination angle λ_s , which can be substituted into (12). The gradient vector \mathbf{g} is then transformed to $\tilde{\mathbf{g}}$ following the above mentioned rule (transformation of unit vectors from c.s. 1 to c.s. 4 by

$\mathbf{T}_{4,1}$), or alternatively it can be expressed by the transformation matrix $\mathbf{T}_{4,0}$ as

$$\tilde{\mathbf{g}}(x, z) := \mathbf{T}_{4,1}(x, z) \mathbf{g}(x, z) = \mathbf{T}_{4,0}(x, z) \begin{bmatrix} 0 \\ 0 \\ 1 \end{bmatrix}, \quad (15)$$

Note that for orthogonal cutting ($\alpha_n = \lambda_s = \eta = 0$) the transformations simplify to $\mathbf{T}_{4,0} = \mathbf{R}_{2,\varphi} \mathbf{R}_{3,-\pi/2}$ (and $\mathbf{T}_{4,1} = \mathbf{I}$), and (15) degrades to $\tilde{\mathbf{g}} = \mathbf{g}$, as expected.

The uncut chip thickness is equal to the length of the streamline measured on the reference plane, and can be calculated numerically by solving the differential equation

$$\frac{dx}{dz} = \frac{g_x(x, z)}{g_z(x, z)}. \quad (16)$$

Many numerical software provide built-in algorithms to generate streamlines starting from arbitrary points if the vector field is known (e.g., the `streamline` or `stream2` functions in MATLAB). Finding the starting points attached to the cutting edge and end points located on the free boundaries, the length of the path can be determined, which is identical to h .

A demonstration calculation is shown in Fig. 4 related to a rhombic insert with $\kappa_r > 90^\circ$ and with a small nose radius. This was one of the triggering example to create a feasible discretization of the cutting edge that is viable for different feeds. One can follow, by using the curved uncut chip thickness model, how the experienced common chip flow direction is actually rising for larger feeds. Also, different chip flow zones (Fig. 4b,c) can be identified according to the types of interconnections between the present cut, past cut and free surface segments defined along the curved uncut chip area. In the simple cut zone I (Fig. 4c) only the present cut determines directly the chip formation. In the regenerative cut zone II the past cut has a direct effect on the chip formation besides the present cut. The material in zone III and IV is removed basically without clear cutting. In this way, the material is partially deformed away or just carried by the actual already cut chip segments. This actually creates an additional modeling problem, namely, at what level these 'not cutting' zones contribute to the cutting force itself. In this work we rather took cases where this problem does not appear, and simply do not take into account the force contribution of these special 'not cutting' zones.

Consequently, the cutting force (in zones I&II) is distributed along the curved chip thickness, the total cutting force is obtained by summing up the elementary forces over the entire uncut chip area A . In this manner, the cutting force is theoretically written as

$$\mathbf{F} = \int_{(A)} \mathbf{T}_{4,0} \begin{bmatrix} \Lambda_v(a, h) f_v(h) \\ 0 \\ \Lambda_u(a, h) f_u(h) \end{bmatrix} dA, \quad (17)$$

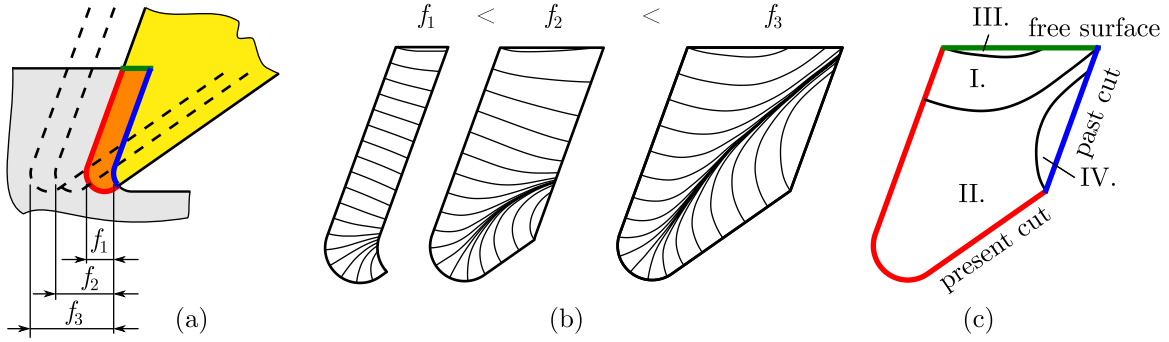


Fig. 4. Feed dependency of the curved uncut chip segments. (a) A rhombic V-type turning insert and the uncut chip area at different feeds. (b) Curved uncut chip thickness at different feeds. (c) Different regions distinguished depending on the start and end points of the curves: I: starts from the present cutting edge and ends in the free edge; II: starts from the present cutting edge and ends in the past cutting edge; III: starts from the free surface and ends in the free surface; IV: starts from the past cutting edge and ends in the past cutting edge.

where $T_{4,0}$ is the local transformation matrix, and h is the uncut chip thickness of the elementary curved chip passing through the infinitesimal chip area dA . Note that the edge coefficients are often modeled as concentrated forces along the edge only. Therefore, by losing generality, we assume that the weight function is of the form

$$\Lambda_j(a, h) := \frac{K_{jc}(h) + K_{je}\delta(a-0)}{K_{jc}(h)h + K_{je}}, \quad j = u, v, \quad (18)$$

where $\delta(a-0)$ is the shifted Dirac-delta function, which indicates that the edge force is defined at the positive side of zero. This definition automatically satisfies (8), moreover

$$\int_0^h \Lambda_j(a, h) f_j(h) da = f_j(h) \quad (19)$$

also holds. Inserting definition (18) into (17) yields

$$\mathbf{F} = \int_{(A)} \mathbf{T}_{4,0} \begin{bmatrix} K_{v,c}(h) \\ 0 \\ K_{u,c}(h) \end{bmatrix} dA + \int_{(L)} \mathbf{T}_{4,0} \begin{bmatrix} K_{v,e} \\ 0 \\ K_{u,e} \end{bmatrix} dL, \quad (20)$$

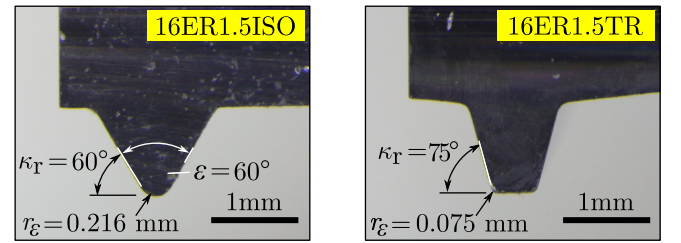
where the second integral is only evaluated along the cutting edge of length L . Note that formula (20) is directly obtained, if the edge coefficient is not considered as part of the characteristics $f_j(h)$. Since the computation of the cutting force defined in the form (20) is not possible analytically in general cases, the numerical integration is written instead in the form

$$\mathbf{F} = \sum_{i=1}^{N_e} \mathbf{T}_{4,0,i} \begin{bmatrix} K_{v,c}(h_i) \\ 0 \\ K_{u,c}(h_i) \end{bmatrix} \Delta A_i + \sum_{j=1}^{N_k} \mathbf{T}_{4,0,j} \begin{bmatrix} K_{v,e} \\ 0 \\ K_{u,e} \end{bmatrix} \Delta L_j, \quad (21)$$

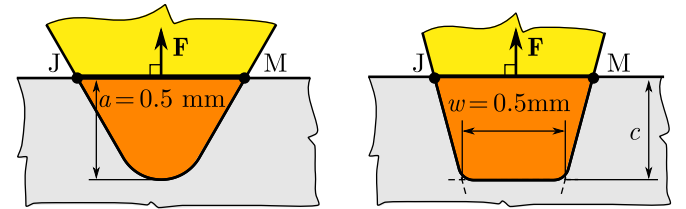
where N_e is the number of discrete elements on the area, h_i is the length of the curved uncut chip segment passing through the center of element numbered i , ΔA_i is the area portion, $\mathbf{T}_{4,0,i}$ and $\mathbf{T}_{4,0,j}$ are the local transformation matrices assigned to the area and edge segments, ΔL_j is the length of the elementary cutting edge, and N_k is the number of the elementary edges. The numerical integration is based on the triangulation of the uncut chip area, which is already available as a result of the finite element meshing (see Appendix A).

2.2. Examples

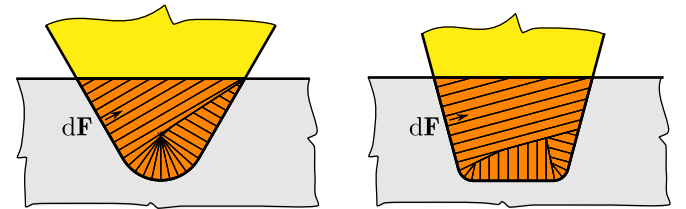
Here, we present some theoretical examples, which are investigated in experiments in Sections 3 and 4. Keep in mind that the models give very close results, when the uncut chip thickness is small (e.g., $h < 0.1$ mm), but the deviation increases for extreme cutting conditions. Two thread cutting inserts are presented (see Fig. 5), which are assumed to create the final shape of the pitch (almost) in one step. Although this operation has minor technical relevance, it can be tested in experiments and can be referred to as a reference setup.



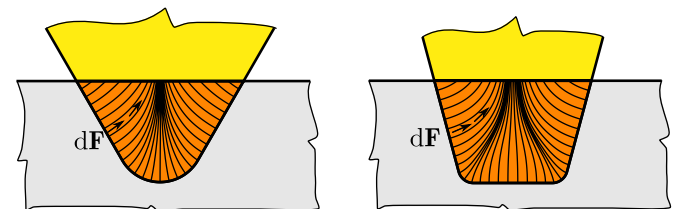
(a) thread turning inserts used in the experiments



(b) Colwell's model



(c) Young's model with chip interference



(d) curved uncut chip thickness model

Fig. 5. Examples for extreme uncut chip geometries. (a) Metric and trapezoidal thread turning inserts. (b) Cutting force direction according to Colwell's method. (c) Straight uncut chip segments and the chip interference problem in Young's model. (d) Curved uncut chip thickness model.

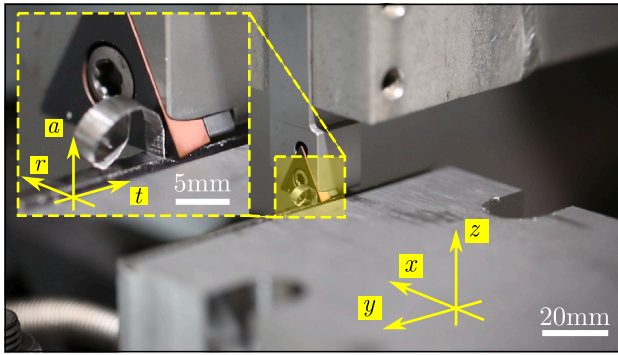


Fig. 6. Laboratory experiments. Chip formation in case of orthogonal cutting on titanium alloy (Ti6Al4V) with a flat insert (TCMW16T304).

Fig. 5a shows a microscopic view of a standard metric thread turning insert of type 16ER1.5ISO (left), and of a trapezoidal thread turning insert of type 16ER1.5TR (right). The metric insert has nose radius $r_e = 0.216$ mm, while the radius of the trapezoidal insert is only $r_e = 0.075$ mm (the geometric data are given in Fig. 5a,b). In this study, the depth of cut is assumed to be $a = 0.5$ mm. It can be seen in the figures how the elementary chip segments are calculated according to Colwell's model (Fig. 5b), Young's model (Fig. 5c), and curved uncut chip thickness model (Fig. 5d). In such extreme depth of cuts, Young's method produces self-intersections (chip interference) if all segments are perpendicular to the edge (the rightmost are chopped off now). *The partitioning is not even symmetric in this case, which is definitely not correct considering the symmetric nature of the problem.* Therefore, Young's method cannot be applied without significant modifications (one alternative approach is presented by Khoshdarregi and Altintas [4]). The curved uncut chip thickness model, however, gives a smoother transition without producing interference in a complete mathematical consistency, moreover, the segments are more realistic.

Considering only the geometries above, one can conclude that (especially for liner cutting force characteristics) Colwell's method gives the largest cutting force, since the magnitude is proportional to the uncut chip area. As opposed to this, Young's method always generates segments that point partially toward each other, therefore the total force is reduced. The prediction of the curved uncut chip thickness model is found somewhere between the other two, since the trajectories start similarly to Young's method, but point outwards at the free surface (as Colwell suggested). Also note that the tangential forces (especially for orthogonal cutting) are practically identical for the different models, because the elementary normal force vectors are all parallel and the magnitude of the tangential force is closely proportional to the uncut chip area.

3. Laboratory experiments

Laboratory experiments are carried out for a titanium alloy Ti6Al4V (grade 5), which is a widely used material in aerospace industry. Machining of these materials is very complicated due to their high chemical activity and poor thermal conductivity resulting high cutting temperatures [41]. In order to extend tool life, tool manufacturers recommend different cutting speed zones for different machining operations, for instance, $v_c = 20 - 25$ m/min for first stage machining (e.g., heavy roughing or skin removal). However, in some literature studies where the aim was to test scientific concepts, the cutting speed is even below this, in the range of $3 - 6$ m/min [42]. Nowadays, for intermediate stage machining operations (e.g., profiling), the cutting speeds are in the range $v_c = 40 - 80$ m/min, but these operations are often performed with coolant.

Experiments are performed on an NCT EmR-610Ms milling machine, which is extended by a tool clamping adapter to perform planing

(shaping) operations. The cutting speed was $v_c = 21$ m/min for all of the tests and no cooling was applied. The speed was technologically limited by the highest speed of the machine, however, it falls into the domain of technologically accepted region for titanium alloys. Moreover, there are operations like broaching in aviation industry, where the cutting speeds are limited to this or to an even smaller regions, see the work of Axinte and Gindy [43] ($v_c \approx 4.05 - 4.8$ m/min).

A schematic of the cutting test experiments can be seen in Fig. 6. The operations were linear planing done on a raw block of workpiece, which was fixed onto a Kistler 9129AA multi-component dynamometer. The data were acquired by NI-9234 input modules and an NI cDAQ-9178 chassis. The length of the machined side of the block was 100 mm.

3.1. Identification of cutting force characteristics

The cutting force characteristics have been identified from cutting tests performed on premachined ridges (the width of the ridge is $b = 2$ mm, see Fig. 6).

During the tests TCMW16T304 carbide inserts were used, a schematic view of the configuration is seen in Fig. 7b. Classical orthogonal cutting models assume that the elementary uncut chip segments are normal to the cutting edge and the uncut chip thickness is equal to the prescribed feed in the axial direction, see Fig. 7c. As opposed to this, the curved uncut chip thickness model produces a minor side flow effect close to the sides only, see Fig. 7d, which can be also related to burr forming. However, it has negligible effect on the cutting forces if the prescribed feed is much smaller than the ridge width. Therefore we can omit the curved uncut chip thickness model here, and apply the classical models instead, with assuming that the feed is equal to the uncut chip thickness h . During the measurements, the feed was varied non-uniformly from 0.005 to 0.3 mm (e.g., $h = 0.005, 0.01, 0.02, 0.03, 0.04, 0.05, 0.06, 0.07, 0.08, 0.09, 0.1, 0.125, 0.15, 0.175, 0.2, 0.225, 0.25, 0.275$ mm) to obtain the specific cutting forces $f_j(h)$.

In order to make sure that tool wear did not initiate during the experiment and the prescribed uncut chip thickness was accurate, all of the tests have been repeated four times at a fixed uncut chip thickness h , see Fig. 7a. The zeroth test was dropped due to the possible static deformations originating from the surface location errors. The prescribed uncut chip thickness was correct after the zeroth test, and tests 1-2-3 were used to check the convergence (and repeatability). If the mean cutting forces were (closely) the same, it means that the conditions did not change (e.g., deformation or tool wear). If the static deformation is significant, then the forces tend to increase from test to test. Similarly, if tool breakage or tool wear initiates, then the forces diverge. In case of signs of tool wear, the insert was replaced and the tests were continued. Furthermore, cutting tests were regularly repeated at $h = 0.05$ mm in order to make sure that the forces are invariant. When tool wear initiates, the cutting force components change (sometimes radically) and this change is monitored by repeating the same tests at a fixed uncut chip thickness ($h = 0.05$ mm). If the mean forces were approximately the same (below a threshold of 5%), then the experiment was continued. The accepted measured mean cutting forces are indicated in Fig. 8a.

The uncut chip thickness was also changed randomly between different test cuts below $h = 0.2$ mm. The mean forces show a smooth monotonic tendency indicating that the order of test cuts did not affect the results. Above $h = 0.2$ mm the measured forces were evaluated cautiously, because the heat generated during cutting was large and the edge damage initiated suddenly. When the difference was larger than the limit, the insert was either replaced (and the test was repeated) or the test series was finished. The largest uncut chip thickness, above which the tool wear was always significant are indicated by crosses in Fig. 8. These last measurement points (crosses) should not be considered during the evaluation, but they show how the evolving tool wear affects the forces.

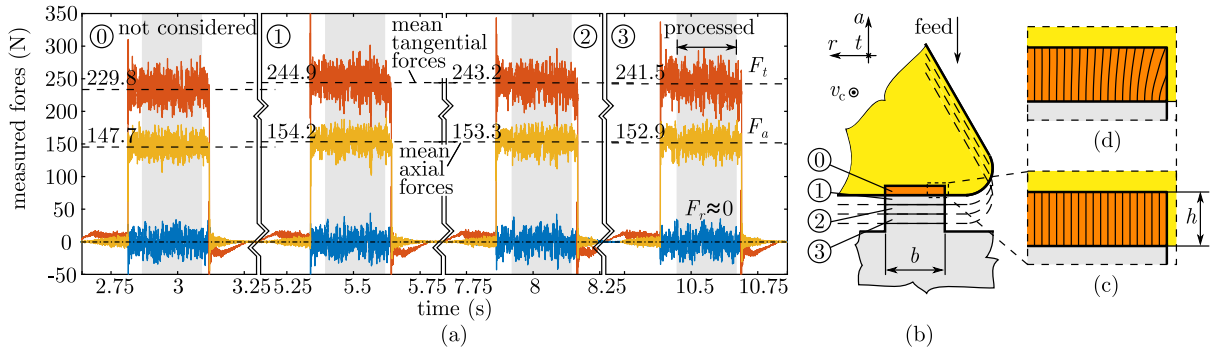


Fig. 7. Raw (unfiltered) measurement data (cutting forces) in orthogonal cutting on titanium alloy (Ti6Al4V) with a flat insert (TCMW16T304) at uncut chip thickness $h = 0.05$ mm. (a) Four subsequent cutting tests are performed on the top of the premachined ridge (ridge width is $b = 2$ mm). The zeroth test is not considered during the evaluation due to the possible static deformations that lead to deviating results. (b) Schematic view of the uncut chip area and cutting steps 0-3. (c) Classical orthogonal cutting models assume that the elementary chip sections are perpendicular to the cutting edge and the uncut chip thickness h is equal to the feed in the axial direction. (d) The curved uncut chip thickness model produces a minor side flow effect close to the sides only. This effect is negligible if the feed is much smaller than the ridge width, but can be also related to burr forming.

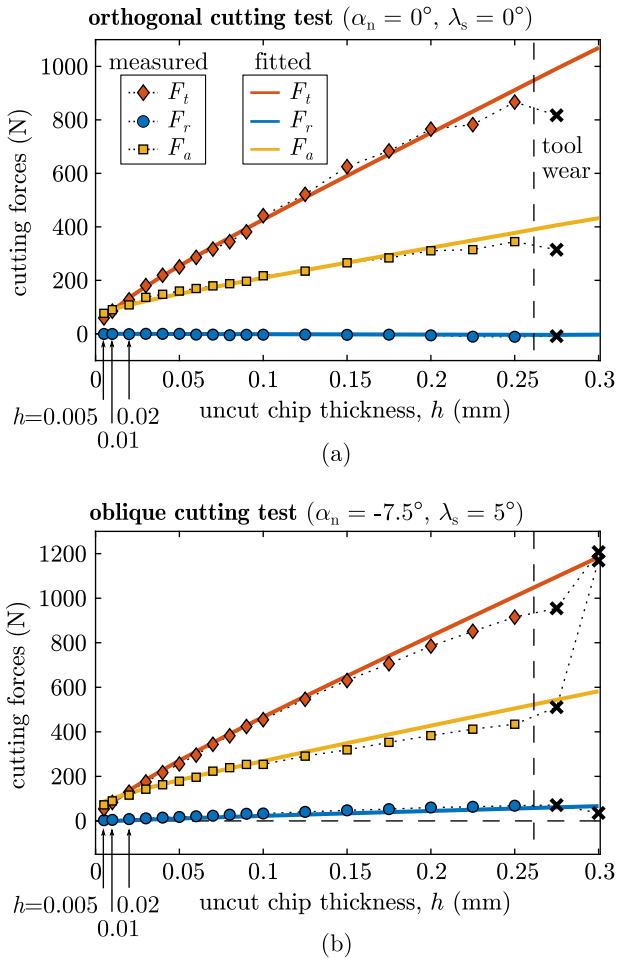


Fig. 8. Orthogonal and oblique ridge cutting tests on titanium alloy (Ti6Al4V) with a flat insert (TCMW16T304). Measured and fitted force components in (a) orthogonal and (b) oblique cutting (ridge width is $b = 2$ mm).

The same measurement procedure has been conducted for a different tool holder (with the same insert) in order to analyze the variation of technological parameters. The rake and inclination angles of the setup were $\alpha_n = -7.5^\circ$ and $\lambda_s = 5^\circ$. The cutting forces are shown in Fig. 8b.

Table 1

Fitted cutting parameters for titanium alloy (Ti6Al4V), where β_a and α_n are given in radian and h is given in mm [3].

$\tau_s = 613$ MPa	$C_0 = 0.88 + 0.63\alpha_n$ (rad)
β_a (rad) = $0.34 + 0.441\alpha_n$ (rad)	$C_1 = 0.35 + 0.12\alpha_n$ (rad)
$r_c = C_0 h(\text{mm})^{C_1}$	$K_{uc} = 32.34$ N/mm
$\phi_a = \arctan \frac{r_c \cos \alpha_n}{1 - r_c \sin \alpha_n}$	$K_{vc} = 4.6$ N/mm

The force model presented by Altintas [3] for titanium alloys was adopted, and the parameters were tuned according to the measurements. The shear angle $\phi_n(h)$ was assumed to depend on the uncut chip thickness h , which makes the cutting coefficients $K_{uc}(h)$ and $K_{vc}(h)$ dependent on h . A nonlinear iterative curve fitting technique has been used, and the sum of the square of the errors of the forces has been minimized. Due to its small effect, we can omit the curved uncut chip thickness model here ($h \ll b$, the assumed chip flow direction is axial), and use only the classical orthogonal to oblique transformations presented in Section 1.3. Therefore, the variables tuned during the fitting process were τ_s , K_{uc} , K_{vc} , β_a , C_0 , C_1 , where the last three (β_a , C_0 , C_1) were assumed to be linear functions of α_n with two parameters [3]. The obtained data are given in Table 1, and the fitted characteristics are indicated by solid colored curves in Fig. 8.

In the rest of the work, experimental cutting force test and predictions are compared using the identified characteristics. The test inserts are later replaced by thread turning inserts in order to present more extremely cutting operations, but the identified cutting parameters were not changed. Experiments showed good agreement (especially at small uncut chip thickness) with predictions, meaning that the characteristics needed no change.

3.2. Cutting tests with rounded tool

Two orthogonal and two oblique cutting test series have been conducted on the same experimental configuration (Fig. 6). The procedures were the same, the tests were stopped when the tool wear initiated.

The static compliance of the tool holder design was important in these tests, because the deformation in direction x results in change in the actual depth of cut, as opposed to the ridge tests. The cuts were repeated four times with the same feed in direction z , therefore the deformation in this direction was compensated. The static compliance C of the tool at the tool tip was identified from dynamical impact tests using a modal hammer (Endevco 2302-10), accelerometers (PCB 352C23), and the NI data acquisition system. The measured compliance matrix C of the assembled tool and clamping device (obtained after

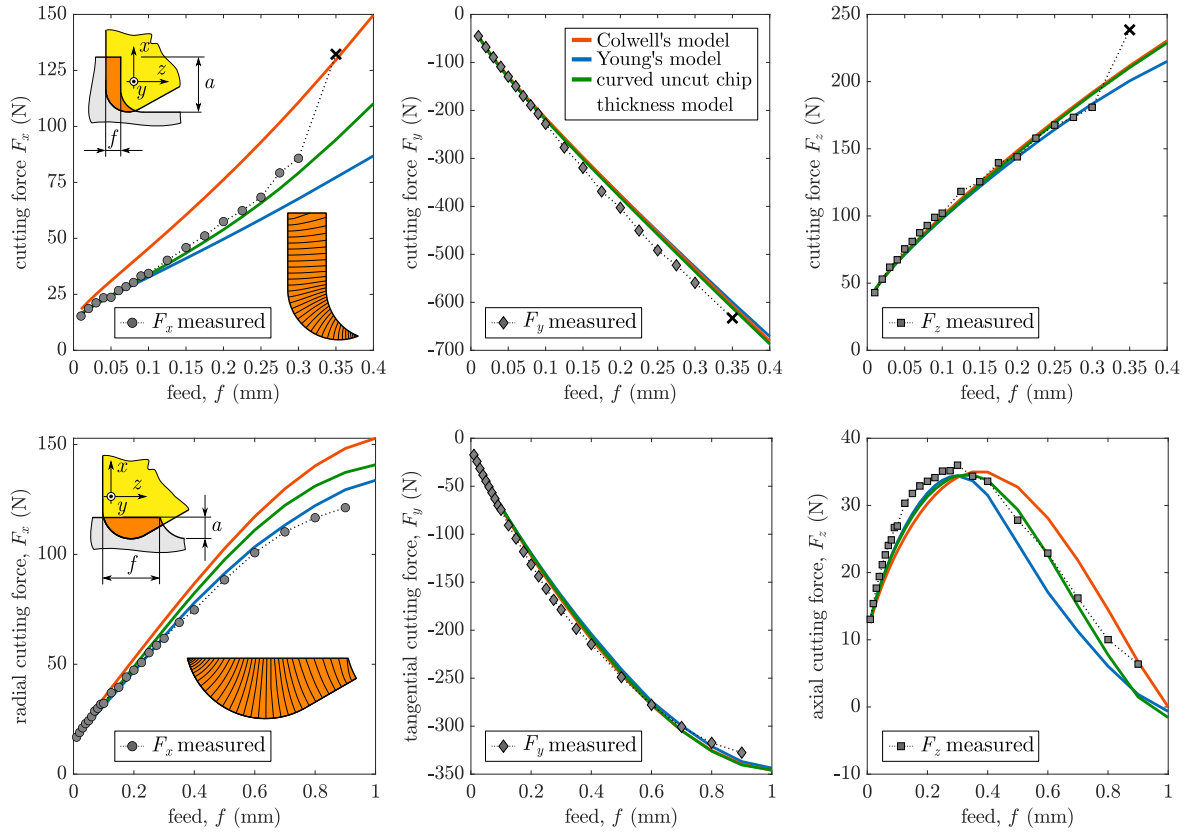


Fig. 9. Cutting force validation on titanium alloy (Ti6Al4V) with a flat insert (TCMW16T304). Parameters are $\kappa_t = 90^\circ$, $\gamma_t = 0^\circ$, $\gamma_p = 0^\circ$, $\varepsilon = 60^\circ$, $r_e = 0.4$ mm, the dept of cuts are (a) $a = 1$ mm and (b) $a = 0.3$ mm.

post-processing the data) corresponding to the tool tip in the (x, y, z) coordinate system (see Fig. 6) is

$$\mathbf{C} = \begin{bmatrix} 0.1405 & -0.0172 & -0.0834 \\ -0.0172 & 0.0067 & 0.0076 \\ -0.0834 & 0.0076 & 0.0531 \end{bmatrix} \cdot 10^{-6} \frac{\text{m}}{\text{N}}. \quad (22)$$

The actual depth of cut can be calculated by solving a nonlinear algebraic equation

$$\Delta \mathbf{r} = \mathbf{C} \mathbf{F} (a - \Delta r_x), \quad (23)$$

where $\Delta \mathbf{r} = [\Delta r_x, \Delta r_y, \Delta r_z]^T$ is the vector of static deformations of the tool tip resulted by the cutting force \mathbf{F} . When the stiffness is large, a few iterations (5–10) converge, which results in 5%–10% difference in the cutting force. However, this small change also affects the final characteristics and the comparisons.

The predicted and the measured cutting forces are presented in Fig. 9. It shows two orthogonal cutting operations, where the prescribed depth of cuts are $a = 1$ mm and $a = 0.3$ mm, respectively. The feed f was increased until the tool wear initiated and the procedure could not be continued. The same cutting operation was repeated with an oblique tool holder, the results are shown in Fig. 10. In each case, the predicted forces (according to Colwell's model [18], Young's model [24] and the curved uncut chip thickness model) were compared to the measured forces. The cutting forces F_y (tangential) in Figs. 9 and 10 are the largest in magnitude, however, the different models predict similar values. As opposed to this, the cutting forces F_x and F_z are sensitive to modeling approaches, meaning that the predictions tend to diverge at higher feeds. Accurate prediction of F_x and F_z has a huge impact on the machine's precision, static deformation and dynamic properties in case of (internal) turning operations.

Due to the limited feeds and depth of cuts, it was not possible to reach higher material removal rates and show significant differences

without tool damage. The last cut at the highest feeds resulted in significant tool wear in a single cut, which prevented further tests. The difference between the models is moderate, the predicted F_y is typically less distinguishable compared to the measured values, however, the other two force components (F_x and F_z) carry higher differences both in relative and absolute value depending on the uncut chip area (Figs. 9 and 10). In most of the cases the measured force components F_x and F_z tend to lean toward the predicted forces of the new proposed method. However, the measurement methodology can only assure that Colwell's approach is the least accurate. Young's method and the new curved uncut chip thickness model compete to be the most accurate prediction. This is not surprising, since for achievable cutting conditions Young's method can reconstruct the force quite well, the argument here is that for these cases, the new uncut chip thickness method can serve predictions with the same accuracy without running into any inconsistency.

3.3. Metric thread turning insert

Since the tool damage could not be prevented at higher feeds, it was not possible to continue the experiments on titanium alloy with the insert TCMW16T304. Instead, a 16ER1.5ISO external metric threading turning insert has been applied, which has a nose radius $r_e = 0.216$ mm (smaller than the previous insert having $r_e = 0.4$ mm). With this insert, the configuration presented in Section 2.2 can be tested. The surface of the insert was flat, however, the normal vector was not completely parallel with the cutting velocity vector, meaning that the cutting operation is not purely orthogonal, the cutting edge angles were $\gamma_t = -0.8^\circ$ and $\gamma_p = 1.2^\circ$. The predicted and measured cutting forces are presented in Fig. 11. It must be noted that the predicted cutting force components F_x and F_z give good agreement with measurements, but

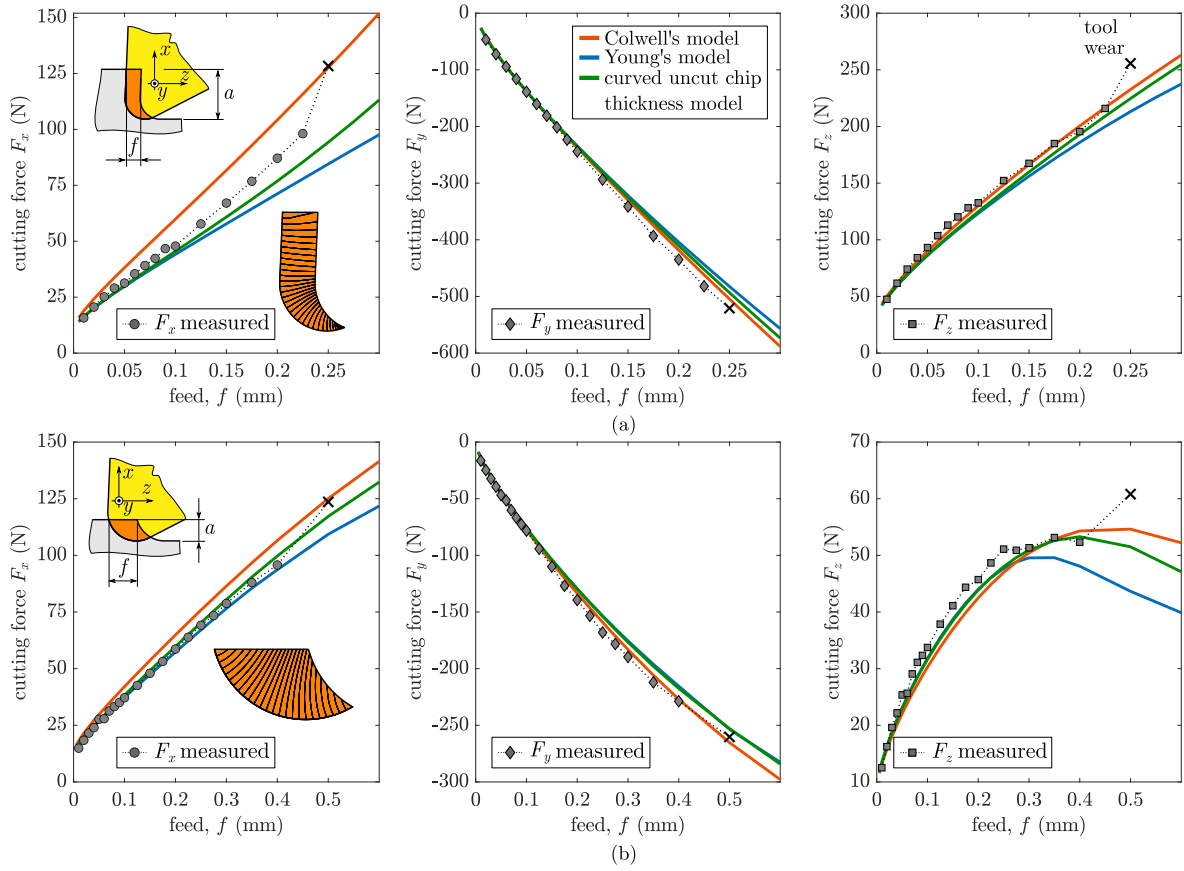


Fig. 10. Cutting force validation on titanium alloy (Ti6Al4V) with a flat insert (TCMW16T304). Parameters are $\kappa_r = 93^\circ$, $\gamma_t = -7.5^\circ$, $\gamma_p = -5^\circ$, $\epsilon = 60^\circ$, $r_e = 0.4$ mm, the dept of cuts are (a) $a = 1$ mm and (b) $a = 0.3$ mm.

the tangential force F_y tends to underestimate the actual force a bit. In the cutting test series, the depth of cuts were $a = 0.2$ and $a = 0.3$ mm. At $a = 0.4$ mm the tool tip again damaged and experiments could not be continued.

3.4. Trapezoidal thread turning insert

Laboratory experiments were extended by trapezoidal thread cutting tests. The type of the used insert was 16ER1.5TR (DIN 103), which implies higher difference in the cutting force predictions due to its shape. The radius is only $r_e = 0.075$ mm, which means that at depth of cuts higher than the radius, Young's model is violated. An example on the shape of the elementary curved uncut chip segments is presented in Section 2.2 (Fig. 5c).

Since the experimental tests were linear planing, the tool path had to be designed in a way, which is ideal for the turning insert. In other words, in order to make sure that the flank face does not rub on any side of the tool (the local clearance remains positive), the radial feed velocity must be set according to the recommendations given in the catalog. The thread turning insert is placed into a standard tool holder, with an anvil below the insert. The tool was moved along an inclined straight path, so the angle between the cutting velocity vector and the normal vector of the rake face was 1.7° . Therefore, the equivalent rake angles in the model are $\gamma_t = 1.7^\circ$ and $\gamma_p = 0^\circ$ (oblique cutting).

The measurement results are shown in Fig. 12. The predictions correlate well with the measurements even above the depth of cut $a = 0.2$ mm. The value of the actual corner radius does not affect significantly the predictions (ideally, it can be set to zero), since it is much smaller than the depth of cut. However, note that theoretically Young's model is not valid above feed $f = 0.1$ mm, due to inconsistency

(interference). It can also be seen that the axial force is not even correct, because the uncut chip area is not divided into symmetric portions.

The highest depth of cut, which could be reached during the experiment was $a = 0.45$ mm, because all test inserts have been significantly damaged at $a = 0.5$ mm. This could be seen on the cutting force signals, but visual inspections also verified it. Significant tool wear often resulted in elevated cutting forces, as seen in the figure (false measurement points are indicated by crosses).

4. Industrial experiments

Laboratory cutting force validations were limited in terms of cutting speed, forces and performance. Therefore, industrial tests have also been performed on heavy-duty lathe machine (NCT EEN-630), which could reach the domain of extreme cutting parameters.

A flat TCMW16T304 turning insert was used, and the workpiece was made of a commercial carbon steel. Since the exact cutting characteristics could not be taken from references, first, orthogonal cutting tests have been performed on premachined ridges. The width of the ridge was $b = 1.6$ mm, the initial diameter of the workpiece was $D = 175$ mm, and the spindle speed was in the region 200–230 rpm keeping the cutting speed $v_c = 110$ m/min during the tests. The measured forces are indicated by markers in Fig. 13. The highest uncut chip thickness, which could be reached was $h = 0.6$ mm. This is significantly higher than what regular papers publish, and this study showed that the characteristics can be extended to high uncut chip thickness values. The results were not reliable above $h > 0.6$ mm due to strong segmentation and fluctuations in the cutting forces.

The fitted nonlinear cutting force characteristics is given in the form $f_u(h) = K_{uc}(h)h + K_{ue}$ and $f_v(h) = K_{vc}(h)h + K_{ve}$, where $K_{uc}(h) = 35.8h^{-0.4499}$ MPa, $K_{ue} \approx 0$ N/mm, $K_{vc}(h) = 54.12h^{-0.1687}$ MPa, and

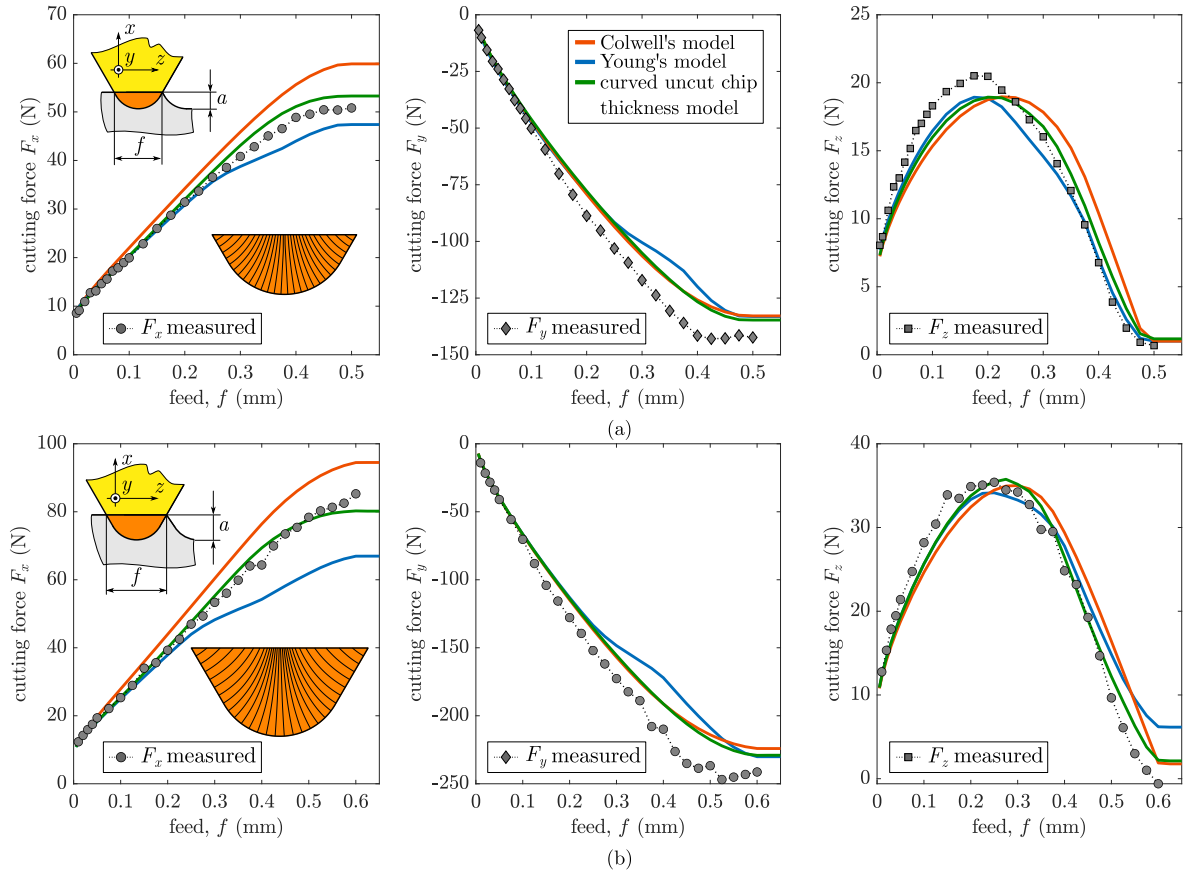


Fig. 11. Cutting force validation on titanium alloy (Ti6Al4V) with a metric thread cutting insert (16ER1.5ISO). Parameters are $\kappa_r = 60^\circ$, $\gamma_r = -0.8^\circ$, $\gamma_p = 1.2^\circ$, $\epsilon = 60^\circ$, $r_e = 0.216$ mm, the dept of cuts are (a) $a = 0.2$ mm and (b) $a = 0.3$ mm.

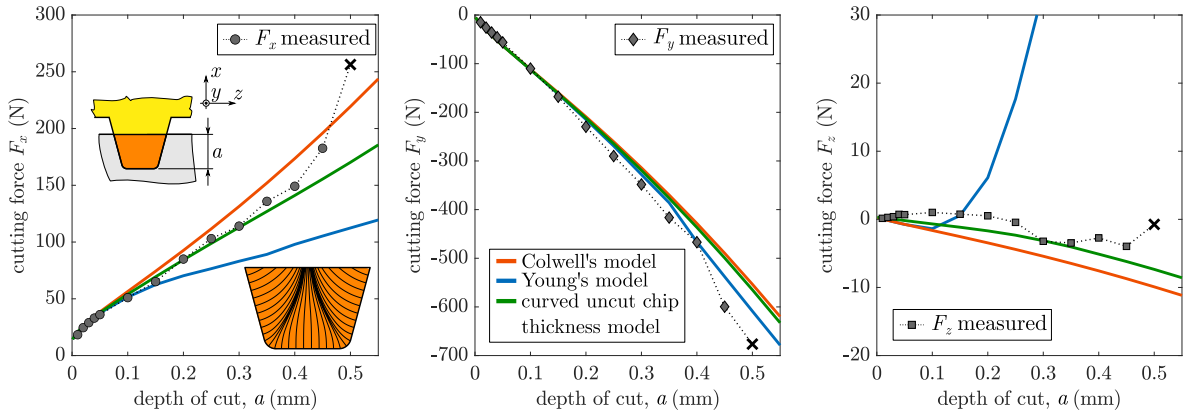


Fig. 12. Cutting force validation on titanium alloy (Ti6Al4V) with a trapezoidal thread cutting insert (16ER1.5TR). Parameters are $\kappa_r = 75^\circ$, $\gamma_r = 1.7^\circ$, $\gamma_p = 0^\circ$, $\epsilon = 105^\circ$, $r_e = 0.075$ mm, (geometric data are given in Fig. 5), the dept of cut has been increased until $a = 0.5$ mm.

$K_{ve} = 20.35$ N/mm. This nonlinear cutting characteristics is often used for steels, and in this scenario it gave an accurate characterization.

Facing operations are planned for validation purposes. The depth of cut was fixed to $a = 1$ mm, while the feed per revolution was increased from $f = 0.05$ mm to $f = 1.7$ mm. The angle between the cutting force vector and the normal vector of the rake face was $< 0.2^\circ$, therefore the cutting operation was approximated as an ideal orthogonal cutting process (oblique ridge cutting tests have not been performed).

The predicted and measured cutting force components can be seen in Fig. 14. It is important to note that here only one measurement was performed at a given feed, therefore the uncertainty is higher than in the laboratory tests, where the repeatability was carefully

checked. It can be seen that the measurement points are slightly scattered, and more experiments would be needed to give a confident conclusion. Even though the uncertainties, Young's model produces chip interference above $f \gtrsim 0.5$ mm, meaning that the prediction are not reliable above it. The curved uncut chip thickness model predicts better the turning point (maximum) in the cutting force F_z (axial), which is the most sensitive to modeling concepts in this configuration. The measured cutting force F_x (radial) is, however, rather in between Young's model and the curved uncut chip thickness model. The cutting force F_y (tangential) is the largest in magnitude, but it is still predicted well by all methods. These small discrepancies seem to be the result of modeling error and uncertainties, which are very hard to reduce

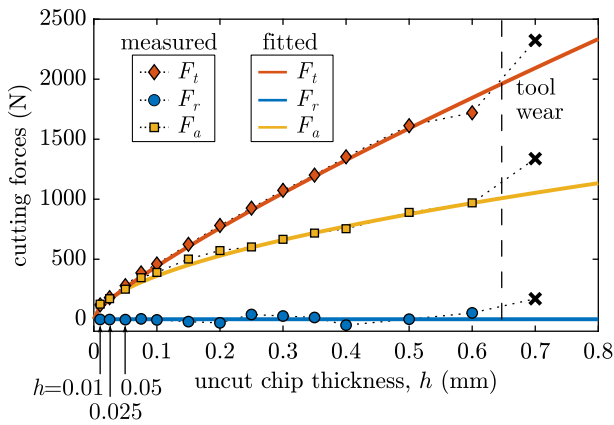


Fig. 13. Orthogonal ridge cutting tests on a carbon steel workpiece. Measured and fitted force components in orthogonal cutting on a premachined ridge (the ridge width is $b = 1.6$ mm).

further. In overall, it can be concluded that the curved uncut chip thickness model gives a generally acceptable result, and it produces no inconsistency in predictions.

5. Conclusion

Current state-of-the-art models do not provide a general framework for cutting force predictions, which lead to problems in case of complex cutting edge geometries. The aim of the research is to establish a generalized but a computationally effective geometric model using the engineering database and uncut chip geometry only. The proposed concept of the curved uncut chip thickness model is based on the classical assumptions, but it distributes the forces along curved paths. The applicability of the method is presented in laboratory experiments (titanium alloy) and in an industrial case study (carbon steel). The main results and findings are summarized as follows.

- The curved uncut chip thickness model cooperates with the orthogonal to oblique transformation and with general empirical cutting force characteristics. Moreover, special tool profiles and complex cutting edge geometries can be handled numerically without any difficulty.
- The curved uncut chip segments are generated from a vector field, which intends to mimic the motion of the chip material grazing the rake face. These segments do not overlap each other, i.e., the solution is free of inconsistency.
- The vector field is obtained by a basic mechanical model (a compressed plate model), which has a unique mathematical solution. This is one trial solution, but the core model should be updated to represent better the elementary force directions. The boundary conditions should be investigated in the future to make a more realistic prediction. Any vector field can be implemented by the model.
- The curved uncut chip thickness model and Young's model give identical solution for small uncut chip thickness, but diverge for high feeds and extreme uncut chip geometries.
- The normal and frictional stress distributions (represented by weight functions A_j) were not investigated in this study. For straight segments, the distributions have no effect on the computation. However, the cutting forces depend on the distributions in case of curved uncut chip segments. This extension is yet an even more challenging problem that needs empirical formulae or simulations, which are sources of additional uncertainties.
- It was found that the experimental validation is difficult due to the extreme cutting conditions. Unmodeled phenomena, changes in friction coefficients, chip segmentation, and heat generation

during chip formation may also affect the validation, which are hard to monitor and/or control.

Advanced multi-physics finite element simulations considering material models and nonlinear phenomena may explain better the chip formation process, however, as mentioned in the introduction, it is significantly more complicated than the use of classical models. It is also important to note that the mechanistic models (Colwell's, Young's, curved uncut chip thickness) cannot predict perfectly the cutting forces for all scenarios, but the advantage is the low computational time with reasonable empirical-based expressions.

It will be of further interest to find a better validation approach, improve the model and also implement it in dynamical simulations.

CRedit authorship contribution statement

David Hajdu: Methodology, Software, Validation, Investigation, Writing – original draft. **Asier Astarloa:** Methodology, Investigation, Writing – review & editing. **Istvan Kovacs:** Investigation, Resources. **Zoltan Dombovari:** Conceptualization, Supervision, Writing – review & editing, Funding acquisition.

Declaration of competing interest

The authors declare that they have no known competing financial interests or personal relationships that could have appeared to influence the work reported in this paper.

Data availability

The data that has been used is confidential

Acknowledgments

The research reported in this paper has been supported by the project EUROSTARS FORTH E!12998, by the Ministry for Innovation and Technology (2019-2.1.2-NEMZ-2019-00005) and by the Hungarian National Research, Development and Innovation Office (NKFI PD-137673).

This research work has been done under the framework of the project MIRAGED: Posicionamiento estratégico en modelos virtuales y gemelos digitales para una industria 4.0 (CER-20191001), supported by CDTI-acreditación y concesión de ayudas destinadas a centros tecnológicos de excelencia cervera.

Appendix A. Finite element model

It is important to note that the concept of the curved uncut chip thickness model is based on the use of a continuous vector field, along which the material is assumed to flow. We present one geometrical model to create such a mathematical solution, but more advanced mechanical models can be developed (at the cost of higher computation and complexity).

A simplified finite element model (FE) is presented to replace complicated and time-consuming numerical simulations. The gradient of the displacement field is found to be applicable to predict the local chip flow directions on the reference plane. The details on the FE model are presented below. Description on finite element models are found in many textbooks, for an introductory course, see the book of Steven M. Lepi [44].

To speed up numerical calculation, a wedge-shaped finite element is applied with reduced number of degrees of freedom (simplification originates from the assumption that only uniform compression is allowed). The element is shown in Fig. 15, which has eight degrees of freedom in total. The thickness is constant, and the external load is compression only normal to the plane. The element is parallel with the (x, z) plane, the vertices are denoted by a, b, c, while the bottom and

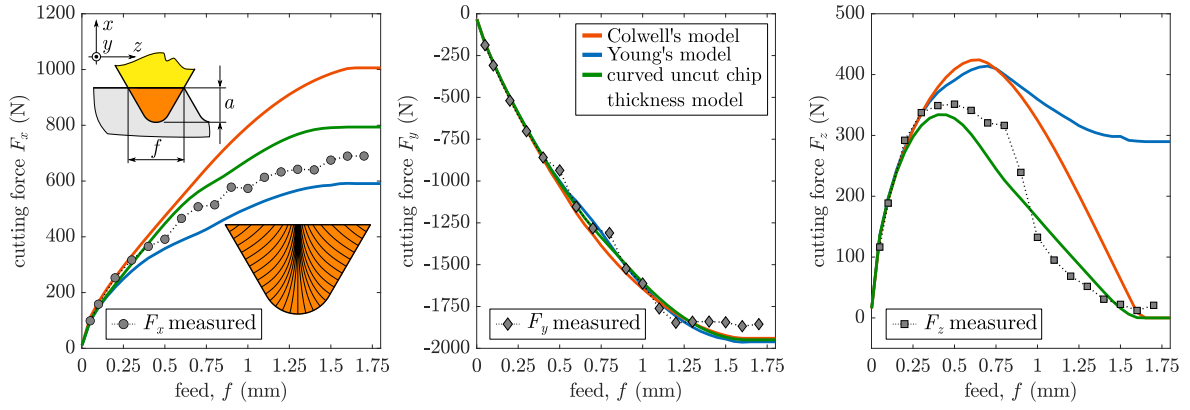


Fig. 14. Cutting force validation on a carbon steel with a flat insert (TCMW16T304). Parameters are $\kappa_r = 60^\circ$, $\gamma_l = 0^\circ$, $\gamma_p = 0^\circ$, $\epsilon = 60^\circ$, $r_e = 0.4$ mm, $a = 1$ mm.

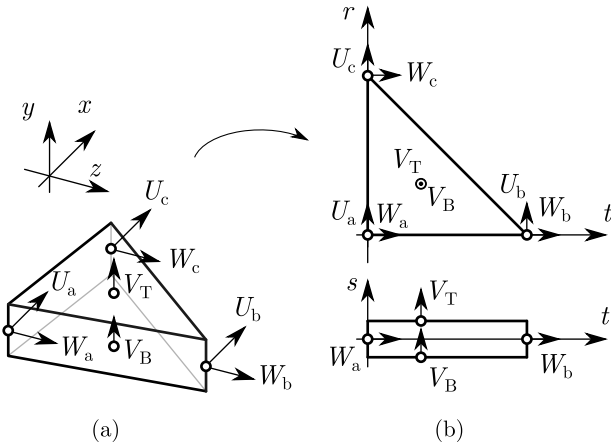


Fig. 15. Triangular finite element used for compression. (a) Global coordinate system. (b) Local coordinate system.

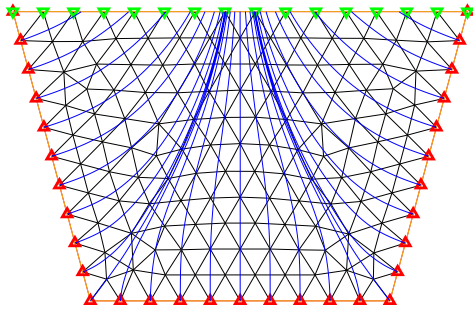


Fig. 16. Output figure of the MATLAB code. Numerical mesh and the curved uncut chip segments generated by the attached code.

top layers by B and T. The nodal displacements are therefore U_a , W_a , U_b , W_b , U_c , W_c , V_B and V_T .

The transformation between the local (x, y, z) and natural coordinate system (r, s, t) is described by the interpolation functions N_i as

$$\begin{aligned} x(r, s, t) &= N_1 x_a + N_2 x_b + N_3 x_c, \\ y(r, s, t) &= N_4 y_B + N_5 y_T, \end{aligned} \quad (24)$$

$$z(r, s, t) = N_1 z_a + N_2 z_b + N_3 z_c,$$

where

$$N_1 = (1 - r - t), \quad N_2 = t, \quad N_3 = r, \quad N_4 = 1 - s, \quad N_5 = s \quad (25)$$

are the shape functions. Note, that the shape functions are linear, the derivatives are constants, so the interpolated stresses and strains are constant inside the element. The same shape functions are used for the interpolation of the displacement fields, i.e.,

$$\begin{aligned} \tilde{U}(r, s, t) &= N_1 U_a + N_2 U_b + N_3 U_c, \\ \tilde{V}(r, s, t) &= N_4 V_B + N_5 V_T, \end{aligned} \quad (26)$$

$$\tilde{W}(r, s, t) = N_1 W_a + N_2 W_b + N_3 W_c.$$

Following the classical approach of finite element modeling, the elemental stiffness matrix can be calculated as

$$\mathbf{K}^e = \int_{(V)} \mathbf{B}^T \mathbf{E} \mathbf{B} dV = \frac{1}{2} \mathbf{B}^T \mathbf{E} \mathbf{B} \det(\mathbf{J}), \quad (27)$$

where \mathbf{B} is the strain–displacement matrix, \mathbf{E} is the material matrix (containing the modulus of elasticity and Poisson's ratio, which is set to 0.45) and \mathbf{J} is the Jacobian matrix [44]. Note that the integration over the volume of the element is expressed explicitly due the linear interpolation functions.

The equilibrium equation for the entire model is formulated as

$$\mathbf{K} \mathbf{U} = \mathbf{F}, \quad (28)$$

where \mathbf{K} , \mathbf{U} , and \mathbf{F} are the global stiffness matrix, displacement vector, and load vector, which are assembled from the elemental matrices. In the model, we compress the plate normal to its plane (perpendicular to y), which is modeled as a constraint (displacement-driven load). Therefore, the elements of \mathbf{U} contain not only zeros and unknowns, but also the prescribed displacements for V_k ($k = 1, \dots, N_e$, N_e is the number of the elements), e.g., 1 and 0 at the top and bottom coordinates, respectively. The inplane deformations U_l and W_l are the unknowns ($l = 1, \dots, N_n$, N_n is the number of the nodes), moreover, the nodes located on the cutting edge are also constrained in direction x and z . Since the equation is linear, the solution is proportional to the load, however, only the gradient of the solution is used, the value of the compression (and material parameters, such as E) is arbitrary.

The nodal displacements U_l and W_l are used to determine the gradient of the displacement field. The norm of the displacement (ignoring the compression in direction y) is calculated as

$$G_i = \sqrt{U_i^2 + W_i^2}, \quad i = a, b, c, \quad (29)$$

and the same interpolation functions are used, i.e.,

$$\tilde{G}(r, s, t) = N_1 G_a + N_2 G_b + N_3 G_c. \quad (30)$$

Using the same procedure, the gradient is calculated from the shape functions and Jacobian matrix as

$$\mathbf{grad} \tilde{G} = \mathbf{J}^{-1} \begin{bmatrix} \frac{\partial N_1}{\partial r} & \frac{\partial N_2}{\partial r} & \frac{\partial N_3}{\partial r} \\ 0 & 0 & 0 \\ \frac{\partial N_1}{\partial t} & \frac{\partial N_2}{\partial t} & \frac{\partial N_3}{\partial t} \end{bmatrix} \begin{bmatrix} G_a \\ G_b \\ G_c \end{bmatrix}. \quad (31)$$

Finally, the vector field can be normalized, and only the projected inplane components are left, i.e.,

$$\mathbf{g}(x, z) = \begin{bmatrix} g_x(x, z) \\ 0 \\ g_z(x, z) \end{bmatrix} := \frac{\mathbf{grad}\tilde{G}}{|\mathbf{grad}\tilde{G}|}, \quad (32)$$

where the component in y is zero due to the simplifications. The artificial displacement gradient $\mathbf{g}(x, z)$ defines the direction of the chip flow on the reference plane.

Appendix B. MATLAB code

A basic MATLAB code is prepared for demonstration purposes, which computes the cutting forces for a simplified tool geometry. In order to make it as short as possible, an orthogonal cutting process is modeled using an ideal trapezoidal thread cutting insert. The cutting force characteristics is assumed to be linear and the edge coefficients are neglected. The output of the Matlab code is shown in Fig. 16. It is important to note that a more general code needs several extensions in order to make it run robustly.

clear all; close all; clc

%TR1.5 trapezoidal thread geometry

a=0.5*10^-3; **%(m) depth of cut**

w=0.5e-3; **%(m) tooth width**

par.Zc=[0 a*sind(15) a*sind(15)+w 2*a*sind(15)+w];

par.Xc=[0 -a*cosd(15) -a*cosd(15) 0];

%cutting coefficients (only linear model)

par.Kuc=500e6; **%(N/m^2) fu(h)=Kuc*h**

par.Kvc=1000e6; **%(N/m^2) fv(h)=Kvc*h**

tic

F=func_cuct_sample(par)

toc

function F=func_cuct_sample(par)

%% FE solution and postprocessing

TR = triangulation(polyshape(par.Zc,par.Xc));

Model = createpde; Tnodes = TR.Points';

Telements = TR.ConnectivityList';

Mesh=geometryFromMesh(Model,Tnodes,Telements);

Mesh=generateMesh(Model,'Hmax',0.5e-4,'GeometricOrder','linear');

pdemesh(Model,'EdgeColor','k'); hold on; axis equal

pdegplot(Model,'EdgeLabels','on'); hold on

FE.FixedNodes=findNodes(Mesh,'region','Edge',[1 3 4]);

FE.FreeNodes=findNodes(Mesh,'region','Edge',[2]);

FE.Elements=Mesh.Elements';

plot(Mesh.Nodes(1,FE.FixedNodes),...

Mesh.Nodes(2,FE.FixedNodes),'r','Linewidth',2)

plot(Mesh.Nodes(1,FE.FreeNodes),...

Mesh.Nodes(2,FE.FreeNodes),'vg','Linewidth',2)

FE.Nodes=1:size(Mesh.Nodes,2);

FE.NodeZ=Mesh.Nodes(1,1:FE.Nodes(end));

FE.NodeX=Mesh.Nodes(2,1:FE.Nodes(end));

FEsol=func_FEsol(FE.Nodes,FE.NodeZ,FE.NodeX,...

FE.Elements,FE.FixedNodes);

[F,Streams]=func_FE_postproc(FE,FEsol,par);

for j=1:size(Streams,2)

plot(Streams{1,j}(:,1),Streams{1,j}(:,2),'-b')

end

end

function FEsol=func_FEsol(Nodes,NodeZ,NodeX,Element,FixedNodes)

DOF=length(Nodes)*2; Ne=size(Element,1); DOFfree=1:DOF;

DOFfree([FixedNodes*2-1 FixedNodes*2])=[];

Er=1; nu=0.45; **%Young's modulus and Poisson's ratio**

VB=0; VT=1; **%bottom and top layers**

E=Er/(1-2*nu)/(1+nu)*[1-nu nu nu 0 0 0;

nu 1-nu nu 0 0 0;

nu nu (1-nu) 0 0 0;

0 0 0 (1-2*nu)/2 0 0;

0 0 0 0 (1-2*nu)/2 0;

0 0 0 0 0 (1-2*nu)/2]; **%3D stress**

for e=1:Ne **%Element matrix**

Xa=NodeX(Element(e,1)); Za=NodeZ(Element(e,1));

Xb=NodeX(Element(e,2)); Zb=NodeZ(Element(e,2));

Xc=NodeX(Element(e,3)); Zc=NodeZ(Element(e,3));

FEsol.Ae(e)=abs(Za*(Xb-Xc)+Zb*(Xc-Xa)+Zc*(Xa-Xb))*0.5;

J11=[-1 0 1]*[Xa Xb Xc].'; J31=[-1 1 0]*[Xa Xb Xc].';

J22=[-1 1]*[VB VT].';

J13=[-1 0 1]*[Za Zb Zc].'; J33=[-1 1 0]*[Za Zb Zc].';

J(:,e)=[J11 0 J13; 0 J22 0; J31 0 J33]; **%Jacobian matrix**

TU=J(:,e)\[-1 0 0 0 1 0 0 0;

0 0 0 0 0 0 0 0;

-1 0 1 0 0 0 0 0];

TV=J(:,e)\[0 0 0 0 0 0 0 0;

0 0 0 0 0 0 -1 1;

0 0 0 0 0 0 0 0];

TW=J(:,e)\[0 -1 0 0 0 1 0 0;

0 0 0 0 0 0 0 0;

0 -1 0 1 0 0 0 0];

B=[TU(1,:); **% eps_x=dU/dx**

TV(2,:); **% eps_y=dV/dy**

TW(3,:); **% eps_z=dW/dz**

TU(2,:)+TV(1,:); **% gam_xy = dU/dy+dV/dx**

TV(3,:)+TW(2,:); **% gam_yz = dV/dz+dW/dy**

TW(1,:)+TU(3,:); **% gam_zx = dW/dx+dU/dz**

Ke(:,e)=B.'*E*B*det(J(:,e))*1/2;

end

%Global stiffness matrix DOF= [u1 w1 u2 w2 ...] [v1 v2 ...];

for e=1:Ne

DOFe=[Element(e,1)*2-1 Element(e,1)*2 Element(e,2)*2-1 ...

Element(e,2)*2 Element(e,3)*2-1 Element(e,3)*2 ...

DOF+e DOF+Ne+e];

[ColDof,RowDof]=meshgrid(DOFe,DOFe);

Cols((e-1)*64+1:e*64)=ColDof(:); Rows((e-1)*64+1:e*64)=RowDof(:);

end

Kg=sparse(Rows,Cols,Ke(:));

Ug0=[zeros(DOF,1);zeros(Ne,1);-ones(Ne,1)]; **%compression it set to -1**

Fg0=-Kg*Ug0; **%Nodal force equivalent to compression**

%Kg condensation and FE solution

Kgc=Kg(DOFfree,DOFfree); Fc=Fg0(DOFfree);

Uc=Kgc\Fc; **%condensed matrix solution**

Ug=zeros(DOF,1); Ug(DOFfree)=Uc;

Ux=Ug(1:2:DOF).'; Uz=Ug(2:2:DOF).';

U=(Ux.^2+Uz.^2).^(1/2); **%displacement vector sum**

gradU=zeros(3,length(Nodes));

for e=1:Ne

FEsol.ucvec(:,e)=J(:,e)\[-1 0 1; 0 0 0; -1 1 0]*U(Element(e,:)).';

gradU(:,Element(e,:))=gradU(:,Element(e,:))+FEsol.ucvec(:,e);

end

FEsol.gradU=gradU./repmat(vecnorm(gradU,2,1),3,1);

end

```

function [F,Streams]=func_FE_postproc(FE,FEsol,par)
Streams=func_streams(FE,...
FEsol.gradU(1,:),'FEsol.gradU(3,:)');
for e=1:size(FE.Elements,1)
dFu(:,e)=par.Kuc*FEsol.ucvec(:,e)*FEsol.Ae(e);
dFv(:,e)=-par.Kvc*FEsol.Ae(e)*[0 1 0];
end
F=sum(dFu+dFv,2); %output force
end

function Streams=func_streams(FE,U,W) %calculation of streamlines
U_interpf=scatteredInterpolant(FE.NodeZ.',FE.NodeX.',U);
W_interpf=scatteredInterpolant(FE.NodeZ.',FE.NodeX.',W);

X_points=linspace(min(FE.NodeX),max(FE.NodeX),101);
Z_points=linspace(min(FE.NodeZ),max(FE.NodeZ),101);
[Zi,Xi]=meshgrid(Z_points,X_points);

W_interp=W_interpf(Zi,Xi); U_interp=U_interpf(Zi,Xi);
Streams = stream2(Zi,Xi, W_interp, U_interp,...
FE.NodeZ(FE.FixedNodes)', FE.NodeX(FE.FixedNodes)');
end

```

References

- [1] P.J. Arrazola, T. Ozel, Investigations on the effects of friction modeling in finite element simulation of machining, *Int. J. Mech. Sci.* 52 (1) (2010) 31–42.
- [2] T. Ozel, I. Llanos, J. Soriano, P.-J. Arrazola, 3D finite element modelling of chip formation process for machining inconel 718: Comparison of FE software predictions, *Mach. Sci. Technol.* 15 (1) (2011) 21–46.
- [3] Y. Altintas, *Manufacturing Automation: Metal Cutting Mechanics, Machine Tool Vibrations, and CNC Design*, second ed., Cambridge University Press, 2012.
- [4] M.R. Khoshdarregi, Y. Altintas, Generalized modeling of chip geometry and cutting forces in multi-point thread turning, *Int. J. Mach. Tools Manuf.* 98 (2015) 21–32.
- [5] H. Li, Z. Xu, Z. Ji, J. Pi, Quantitative characterization of Poisson burrs on the V-shaped texture based on the volume method, *J. Mater. Res. Technol.* 9 (6) (2020) 16280–16288.
- [6] V. Astakhov, *Tribology of Metal Cutting*, Elsevier Science, 2006, p. 392.
- [7] I. Time, *Soprotivlenie Metallov I Dereva Rezanie (Resistance of Metals and Wood to Cutting)*, Dermacon Press House, St. Petersburg, Russia, 1870.
- [8] H. Tresca, *Memoir on the planning of metals*, *Bull. de la Soc. D'Encourag. Pour L'Ind. Natl.* 15 (1873) 585–685.
- [9] I. Time, *Mémoire sur Le Rabotage Des Métaux, Expédition pour la confection des papiers de l'Etat*, 1877.
- [10] K. Zvorykin, On the force and energy needed to separate the chip from the workpiece, *Tekhnicheskii Sbornik I Vestnic Promyslinosty* 123 (117) (1896) 57–96.
- [11] M.E. Merchant, Mechanics of the metal cutting process. I. Orthogonal cutting and a type 2 chip, *J. Appl. Phys.* 16 (5) (1945) 267–275.
- [12] M.E. Merchant, Mechanics of the metal cutting process. II. Plasticity conditions in orthogonal cutting, *J. Appl. Phys.* 16 (6) (1945) 318–324.
- [13] E.H. Lee, B.W. Shaffer, The theory of plasticity applied to a problem of machining, *Trans. ASME J. Appl. Mech.* 18 (1951) 405–413.
- [14] W.B. Palmer, P.L.B. Oxley, Mechanics of orthogonal machining, *Proc. Inst. Mech. Eng.* 173 (1) (1959) 623–654.
- [15] X. Jin, Y. Altintas, Slip-line field model of micro-cutting process with round tool edge effect, *J. Mater. Process. Technol.* 211 (3) (2011) 339–355.
- [16] D. Germain, G. Fromentin, G. Poulachon, S. Bissey-Breton, From large-scale to micromachining: A review of force prediction models, *J. Manuf. Process.* 15 (3) (2013) 389–401.
- [17] J.A. Arsecularatne, P. Mathew, P.L.B. Oxley, Prediction of chip flow direction and cutting forces in oblique machining with nose radius tools, *Proc. Inst. Mech. Eng. B* 209 (4) (1995) 305–315.
- [18] L.V. Colwell, Predicting the angle of chip flow for single-point cutting tools, *Trans. ASME* 76 (1954) 199–204.
- [19] C. Bus, N. Touwen, P. Veenstra, A. van der Wolf, On the significance of equivalent chip thickness, Th Eindhoven. Afd. Werktuigbouwkunde, Laboratorium Voor Mechanische Technologie Enwerkpiaatstechniek : WT Rapporten; VOL. WT0241, Technische Hogeschool Eindhoven, 1970.
- [20] R.S. Hu, P. Mathew, P.L.B. Oxley, H.T. Young, Allowing for end cutting edge effects in predicting forces in bar turning with oblique machining conditions, *Proc. Inst. Mech. Eng. C* 200 (2) (1986) 89–99.
- [21] D.H. Wen, L. Zheng, Z.Z. Li, R.S. Hu, An improved chip flow model considering cutting geometry variations based on the equivalent cutting edge method, *Proc. Inst. Mech. Eng. B* 217 (12) (2003) 1737–1745.
- [22] M. Eynian, Y. Altintas, Chatter stability of general turning operations with process damping, *J. Manuf. Sci. Eng.* 131 (4) (2009) 041005.
- [23] K. Okushima, K. Minato, On the behavior of chip in steel cutting, *Bull. JSME* 2 (5) (1959) 58–64.
- [24] H.T. Young, P. Mathew, P.L.B. Oxley, Allowing for nose radius effects in predicting the chip flow direction and cutting forces in bar turning, *Proc. Inst. Mech. Eng. C* 201 (3) (1987) 213–226.
- [25] J. Wang, P. Mathew, Development of a general tool model for turning operations based on a variable flow stress theory, *Int. J. Mach. Tools Manuf.* 35 (1) (1995) 71–90.
- [26] J.A. Arsecularatne, R.F. Fowle, P. Mathew, Prediction of chip flow direction, cutting forces and surface roughness in finish turning, *J. Manuf. Sci. Eng.* 120 (1) (1998) 1–12.
- [27] G. Totis, M. Sortino, Robust analysis of stability in internal turning, *Procedia Eng.* 69 (2014) 1306–1315.
- [28] F. Kuster, P. Gygax, Cutting dynamics and stability of boring bars, *CIRP Ann.* 39 (1) (1990) 361–366.
- [29] G. Totis, Breakthrough of regenerative chatter modeling in milling by including unexpected effects arising from tooling system deflection, *Int. J. Adv. Manuf. Technol.* 89 (2017) 2515–2534.
- [30] I. Lazoglu, F. Atabey, Y. Altintas, Dynamics of boring processes: Part III-time domain modeling, *Int. J. Mach. Tools Manuf.* 42 (14) (2002) 1567–1576.
- [31] F. Atabey, I. Lazoglu, Y. Altintas, Mechanics of boring processes - Part I, *Int. J. Mach. Tools Manuf.* 43 (5) (2003) 463–476.
- [32] F. Atabey, I. Lazoglu, Y. Altintas, Mechanics of boring processes - Part II - multi-insert boring heads, *Int. J. Mach. Tools Manuf.* 43 (5) (2003) 477–484.
- [33] M. Kaymakci, Z. Kilic, Y. Altintas, Unified cutting force model for turning, boring, drilling and milling operations, *Int. J. Mach. Tools Manuf.* 54–55 (2012) 34–45.
- [34] Q. Wang, H. Lin, Z. Zhang, Prediction of chip flow angle to study the relation between chip flow and ratio of the cutting edge lengths using sharp corner tools, *Int. J. Adv. Manuf. Technol.* 56 (9–12) (2011) 841–855.
- [35] S. Kouadri, A. Bensari, M. Tirenifi, Experimental and theoretical analysis of the chip flow direction in turning using flatted and grooved inserts – impact of the tool rake face geometry, the work material and cutting conditions, *J. Appl. Mech. Eng.* 06 (03) (2017).
- [36] L. Wu, J. Liu, Y. Ren, Z. Yang, G. Wang, J. Sun, J. Song, W. Xu, X. Liu, 3D FEM simulation of chip breakage in turning AISI1045 with complicate-grooved insert, *Int. J. Adv. Manuf. Technol.* (2020).
- [37] W. Cheng, J. Outeiro, J.-P. Costes, R. M'Saoubi, H. Karaoui, V. Astakhov, A constitutive model for Ti6Al4V considering the state of stress and strain rate effects, *Mech. Mater.* 137 (2019) 103103.
- [38] X. Xu, J. Outeiro, J. Zhang, B. Xu, W. Zhao, V. Astakhov, Machining simulation of Ti6Al4V using coupled Eulerian-Lagrangian approach and a constitutive model considering the state of stress, *Simul. Model. Pract. Theory* 110 (2021) 102312.
- [39] S. Afazov, S. Ratchev, J. Segal, Modelling and simulation of micro-milling cutting forces, *J. Mater. Process. Technol.* 210 (15) (2010) 2154–2162.
- [40] G.V. Stabler, The fundamental geometry of cutting tools, *Proc. Inst. Mech. Eng.* 165 (1) (1951) 14–26.
- [41] I. Jawahir, H. Attia, D. Biermann, J. Duflou, F. Klocke, D. Meyer, S. Newman, F. Pusavec, M. Putz, J. Rech, V. Schulze, D. Umbrello, Cryogenic manufacturing processes, *CIRP Ann.* 65 (2) (2016) 713–736.
- [42] B. Aksu, C. Celebi, E. Budak, An experimental investigation of oblique cutting mechanics, *Mach. Sci. Technol.* 20 (3) (2016) 495–521.
- [43] D.A. Axinte, N. Gindy, Tool condition monitoring in broaching, *Wear* 254 (3–4) (2003) 370–382.
- [44] S.M. Lepi, *Practical Guide to Finite Elements*, Taylor & Francis Inc, 1998.